Annual Reviews in Control xxx (xxxx) xxx

Contents lists available at ScienceDirect

Annual Reviews in Control

journal homepage: www.elsevier.com/locate/arcontrol

A review on nonlinear modes in conservative mechanical systems

Alin Albu-Schaeffer [*,a,b], Cosimo Della Santina [a,b]

[a] Institute of Robotics and Mechatronics, German Aerospace Center (DLR), Oberpfaffenhofen, Germany
[b] Department of Informatics, Technical University of Munich (TUM), Germany

A B S T R A C T

This paper discusses the theory of oscillatory normal modes, and its extension to general multi-body mechanical systems. We first review the efforts to generalize modal analysis to the non-linear case. This body of knowledge is vast and spread across several subfields of mathematics, physics, and engineering. We concisely summarize these results, and connect them together using a language familiar to the control theorist. We then propose a direct way of extending nonlinear modes to mechanical systems with a non Euclidean metrics (e.g. robots).

1. Introduction

It is intuitively clear that the ability of mechanical systems to perform efficient oscillatory motions can be massively enhanced by adequately shaping their inertia properties and the potential fields acting on them. This is very well understood for linear systems, where the relationship connecting physical parameters and resulting free oscillations of the mechanical structures is made explicit by the well-established theory of linear modal oscillations.

Investigations performed within disparate fields suggest that the intuition holds true also in the nonlinear case. For example, studies in biology indicate that animals strongly rely on the interplay between their body dynamics and elasticity, to perform periodic tasks in an efficient and effective way (Geyer, Seyfarth, & Blickhan, 2006; Hogan & Sternad, 2007; Roberts & Azizi, 2011; Schaal, Sternad, Osu, & Kawato, 2004). On the technological side, elastic elements have been added to robotic structures, with the aim of matching the motion capabilities observed in animals, with promising results (Della Santina, Catalano, & Bicchi, 2020; Haldane, Yim, & Fearing, 2017; Robinson, Pratt, Paluska, & Pratt, 1999). Despite the abundance of examples, formalizing these insights in the nonlinear case into a general theoretical framework is still an unmatched goal.

On the other hand, the study of nonlinear oscillations has occupied researchers since more than one century, with first relevant developments due to Poincaré (1899) and Lyapunov (1907), just to cite a few. Yet, the focus of most of these works is confined to either weakly nonlinear systems, or interconnections of points of mass coupled through possibly nonlinear potential fields - i.e. systems with constant inertia tensor. Nonetheless, these theoretical results had significant impact in structural dynamics (Avramov & Mikhlin, 2013; Kerschen, Peeters, Golinval, & Vakakis, 2009; Noël & Kerschen, 2017), where finite element methods naturally produce this kind of dynamic models (Oñate, 2013).

Strangely enough, this large body of work did not find yet its way into the more general and practically very relevant class of dynamically coupled rigid bodies - i.e. mechanical system with non Euclidean geometry (Bullo & Lewis, 2004) - with very few and specific exceptions (Albu-Schaeffer, Lakatos, & Stramigioli, 2019; Della Santina, Lakatos, Bicchi, & Albu-Schaeffer, 2019; Lakatos, Friedl, & Albu-Schäffer, 2017; Tedrake, Zhang, Fong, & Seung, 2004; Wang, Bajaj, & Kamiya, 2005). It is the authors believe that the extension of nonlinear modes to this class of systems can be a key ingredient towards a complete understanding of how the structure of natural and robotic bodies can generate robust and effective oscillatory behaviors.

The aim of this work is therefore to make a first step towards connecting the two worlds. To increase our chances of providing an exhaustive treatise on the topic, we narrowed our focus to (almost exclusively) conservative mechanical systems. We considered the entire spectrum of possible oscillatory behaviors within this class, as shown in Fig. 1. Each definition represented there implements a different trade off between regularity of the oscillation (maximum on the left) and capability of describing behaviors presented by complex systems (maximum on the right).

In the first part of this manuscript (Sections 2–6), we survey existing results which appeared in the state of the art of very distant fields of science. We provide definitions, examples, and basic properties. Fig. 2 shows a collection of simple mechanical systems - presenting increasingly complex oscillatory behavior - that we will use as reference for

* Corresponding author at: Institute of Robotics and Mechatronics, German Aerospace Center (DLR), Oberpfaffenhofen, Germany.
E-mail addresses: Alin.Albu-Schaeffer@dlr.de (A. Albu-Schaeffer), Cosimo.DellaSantina@dlr.de (C. Della Santina).

https://doi.org/10.1016/j.arcontrol.2020.10.002
Received 29 July 2020; Received in revised form 5 October 2020; Accepted 5 October 2020

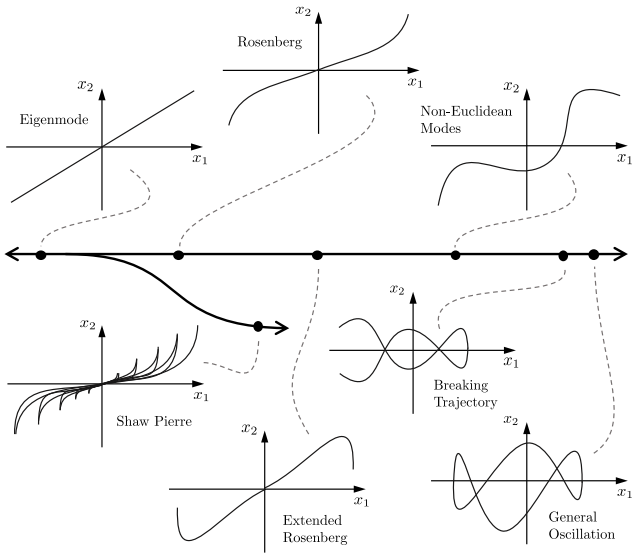

Fig. 1. Principal existing definitions of oscillatory modes. Going from left to right we get to progressively weaker/more general definitions of the concept. At the same time going from right to left we need to constraint more and more the kind of system under consideration - from fully nonlinear to linear - for being able to reasonably expect to find such an evolution. The branch resulting into Shaw-Pierre modes refer to the introduction of damping. All other modes are defined for conservative systems. Similar and strict modes are not reported in the picture since at this level of description they are indistinguishable from eigenmodes and extended Rosenberg modes, respectively.

discussing the various definition. We hope in this way to provide an exhaustive yet concise introduction to the topic from the point of view of control theory and robotics. The second part of the paper (Sections 7–9) is devoted to the extension of nonlinear modes to the dynamically coupled case with non constant inertia tensor. We introduce our definition in Section 7, we discuss how to compute these modes in Section 8, and we show how to describe them through coordinates in Section 9. Finally, Section 10 draws the conclusions and introduces some insights about how nonlinear normal modes can be used in control of mechanical systems.

1.1. Units

Units will often not be explicitly specified in the paper. All physical units may be assumed to be expressed in the MKS system, and angles in radian.

2. Modal analysis for linear systems

We start by looking at the left end of the spectrum reported in Fig. 1. We say that a mechanical system is linear if its configuration space is $\mathbb{R}^n$, the forward kinematics contains only affine functions, and the potential field is quadratic. This corresponds to a set of decoupled masses connected with linear springs. An example of such a system is shown in Fig. 2(a). The time evolutions $x:\mathbb{R}\to\mathbb{R}^n$ of a linear system are all the functions verifying the set of ordinary differential equations (i.e. system dynamics)

$$M\ddot{x}+Kx=0\,, \tag{1}$$

where $M\in\mathbb{R}^{n\times n}$ is the positive definite inertia matrix, $K\in\mathbb{R}^{n\times n}$ is the positive definite stiffness matrix, and $\ddot{x}$ is the second time derivative of x. The energy of (1) is

$$E(x,\dot{x})=\frac{1}{2}\dot{x}^{\mathrm{T}}M\dot{x}+\frac{1}{2}x^{\mathrm{T}}Kx, \tag{2}$$

where $\dot{x}$ is the time derivative of x. Note that for the sake of keeping the notation compact we will use x and $\dot{x}$ to refer both to the whole time evolution, and to a generic value of configuration or velocity. The use will be clear from the context.

Modal analysis of linear mechanical systems is a very well established and widely used tool. We introduce in the following a fully geometric characterization of linear modes and eigenspaces, so to ease the shift to the nonlinear world.

Definition 1. (*Linear modes, adapted from José and Saletan (2000)*) Consider a set of vector spaces $ES_i\subseteq\mathbb{R}^{2n}$, with $i\in\{1\cdots n\}$. We say that ES_i are eigenspaces of (1) if

i) they are invariant w.r.t. (1),
ii) $\oplus_{i=1}^{n} ES_i\simeq\mathbb{R}^{2n}$,
iii) they have dimension 2,

where $\oplus$ is the direct sum of the arguments.

If this is the case, we call normal mode (also eigenmode, oscillatory mode, modal evolution, or just mode) every evolution $x(t)$ such that $(x(0),\dot{x}(0))\in ES_i$.

The two main characterizing properties of linear modes are

a) Invariance: each mode never exits its eigenspace. This is required by hypothesis (i) in Definition 1.
b) Modal superposition: all possible evolutions of (1) can be expressed as linear combination of normal modes. This is direct consequence of hypothesis (ii) and the linearity of (1).

Condition (iii) could have been equivalently framed as: none of the subspaces of ES_i is invariant. This is necessary to assure uniqueness of the definition, at least in the case of distinct eigenvalues of $M^{-\frac{1}{2}}KM^{-\frac{1}{2}}$(non resonance). However, it is not a strongly characterizing property of eigenspaces. Some other important properties of linear modes are: (c) each ES_i can be expressed as direct sum of two subspaces, one lying in the configuration part and the other in the velocity part of $\mathbb{R}^{2n}$; (d) modal evolutions are periodic motions; (e) all modal evolutions within an eigenspace oscillate with a same characteristic frequency; (f) only one orbit exists in each ES_i for any given energy level or amplitude of oscillations; (g) both ES_i and the frequency of oscillation of the associated modes can be evaluated by spectral decomposition of $M^{-\frac{1}{2}}KM^{-\frac{1}{2}}$.

2.1. Example

Consider the system in Fig. 2(a). Its state is $(\dot{x}_1,\dot{x}_2,x_1,x_2)$. Its dynamics can be described by the linear ordinary differential equation

$$m\begin{bmatrix}1+\delta & 0\\ 0 & 1\end{bmatrix}\begin{bmatrix}\ddot{x}_1\\ \ddot{x}_2\end{bmatrix}+k\begin{bmatrix}1+\alpha(\delta+1) & -1\\ -1 & 1+\alpha\end{bmatrix}\begin{bmatrix}x_1\\ x_2\end{bmatrix}=\begin{bmatrix}0\\ 0\end{bmatrix}, \tag{3}$$

where we parametrize stiffnesses as $k_1=\alpha(1+\delta)k, k_2=\alpha k, k_3=k$, and masses as $m_1=(1+\delta)m, m_2=m$, for $\delta>-1, \alpha>0, k>0, m>0$. The two eigenspaces are $ES_1=\mathrm{Span}\{(1,1,0,0),(0,0,1,1)\}$ and $ES_2=\mathrm{Span}\{(-1,1+\delta,0,0),(0,0,-1,1+\delta)\}$, evaluated as prescribed in point (g) of above. They correspond to in-phase and anti-phase oscillations respectively. We evaluate normal modes as complex exponentials of the associated eigenvalues

$$x_2 = +x_1 \Rightarrow x_1(t) = x_1(0)\cos\left(\sqrt{\frac{\alpha k}{m}}t\right),$$

$$x_2 = -(1+\delta)x_1 \Rightarrow x_1(t) = x_1(0)\cos\left(\sqrt{\frac{\left(\alpha+\frac{1}{\delta+1}+1\right)k}{m}}t\right),$$

where the time evolutions are shown for the case of null initial velocity. Fig. 3 contains one example of the in phase normal mode for energy level $\overline{E} = 5$, with $\delta = 0, \alpha = 2, k = 1, m = 1$. Fig. 4 depicts one example of the anti phase normal mode for the same choice of parameters. Both figures also report the oscillation frequency versus the energy. This relation is constant for a linear system, as for property (e) discussed above. Examples of mass movements corresponding to modal evaluations are reported in Fig. 5, this time for $m_1 \neq m_2$. Note indeed that in the anti phase mode the oscillation of m_2 is larger than the oscillation of m_1.

2.2. A note on the dissipative case

Although this is not the focus of the current paper, it is worth remarking that linear modal analysis can easily be extended to the non conservative case (José & Saletan, 2000). Consider the system $M\ddot{x} + Kx = -D\dot{x}$, with $D \geq 0$. Necessary and sufficient condition for it to keep the same modal structure of its conservative counterpart (1), is that $M^{-\frac{1}{2}}DM^{-\frac{1}{2}}$ and $M^{-\frac{1}{2}}KM^{-\frac{1}{2}}$ are simultaneously diagonalizable. This means requiring that $D\dot{x}$ is always collinear with the potential force field Kx. In case this does not happen, it is still possible to generalize the modal decomposition, by allowing for eigenspaces with dimension greater than two.

Interestingly, dissipation often makes the analysis of linear mechanical systems simpler rather than harder. Indeed, even small amount of dissipation rapidly suppresses the higher-frequency modes, practically reducing the motion to only a few of the lowest-frequency modes. This property is particularly relevant in continuous mechanical systems, which have a theoretically-infinite set of normal modes, and instead are in the practice well modelled as evolving in a low-dimensional combination of the slowest modes (De Luca & Siciliano, 1991; Kumar & Narayanan, 2008).

3. Oscillations in nonlinear mechanics

Let us address in this section the right end of the spectrum shown in Fig. 1. Consider a conservative nonlinear mechanical system possibly subject to holonomic constraints, with configuration evolving in a smooth manifold $\mathcal{X}$ of dimension n. This manifold is called configuration manifold. A generic point in $\mathcal{X}$ will be referred as p (see Fig. 23(a)). Endowed with a metric $\mathcal{I}_p$ given by the inertia tensor of the system, $\mathcal{X}$ becomes a Riemannian manifold.

The system velocity v at p is part of the tangent space $T_p\mathcal{X} \simeq \mathbb{R}^n$ (see Fig. 23(b)). The state space of the mechanical system is the tangent bundle $T\mathcal{X}$ of the configuration manifold (roughly speaking, the collection of positions and velocities). More details on notation are provided in the Appendix.

By using the formalism of geometrical classic mechanics (Bullo & Lewis, 2004), the system dynamics can be expressed as

$$\nabla_{\gamma'}\gamma' + \nabla\mathcal{V} = 0, \tag{4}$$

where $\gamma : \mathbb{R} \to \mathcal{X}$ is a trajectory of the system, and $\gamma'(t) \in T_{\gamma(t)}\mathcal{X}$ its associated tangent vector field. The term $\nabla_{\gamma'}\gamma'$ serves as generalization of the acceleration on manifolds, with $\nabla_{\cdot}\cdot$ being the Levi-Civita connection related to $\mathcal{I}_p$. The potential energy of (4) is $\mathcal{V}$, and ∇ is the covariant gradient vector. Therefore $\nabla\mathcal{V}$ are the accelerations due to potential forces. The level sets of $\mathcal{V}$ are $n-1$ dimensional submanifold of $\mathcal{X}$ (see Fig. 23(c)). For the sake of conciseness we consider $\mathcal{V}$ to be positive definite. Therefore, it is assumed that the system has an equilibrium p_{eq} corresponding to the minimum of $\mathcal{V}$. The total energy of (4) is

$$\mathcal{E}(p, v) = \mathcal{K}(p, v) + \mathcal{V}(p), \tag{5}$$

with $\mathcal{K}(p, v)$ being the kinetic energy (see Appendix section for more details). All examples in Fig. 2 fall into the class of systems described by (4). Mechanical systems subject to nonholonomic constraints require more complex models, and will not be considered in this work.

It is always possible to approximate the behavior of any nonlinear system modeled by (4) in a neighborhood of an equilibrium through a linear system expressed by (1). This is called the linearized system (see e.g. (José & Saletan, 2000, Section 4.2.1) or (Bullo & Lewis, 2004, Section 6.2.1)). On a larger scale, we can consider an open set $U \subset \mathcal{X}$, and two charts Φ and $\mathrm{d}\Phi_p$ implementing the parametrization $(p, v) \to (x, \dot{x})$. See Section .3 and Fig. 23(a) and (b) for more details. This yields the usual coordinate expression of (4)

$$M(x)\ddot{x} + C(x, \dot{x})\dot{x} + \frac{\partial V}{\partial x}(x) = 0, \tag{6}$$

where $M \in \mathbb{R}^{n\times n}$ is the positive defined inertia matrix, and $C(x, \dot{x})\dot{x}$ collects Coriolis and centrifugal forces. Together they realize a coordinate dependent version of $\nabla_{\gamma'}\gamma'$, as $\ddot{x} + M^{-1}(x)C(x, \dot{x})\dot{x}$. Similarly, $M^{-1}\partial V/\partial x = \nabla\mathcal{V} \circ \Phi^{-1}$ is the coordinate expression of the accelerations due to potential forces. The total energy of the system expressed in coordinates is

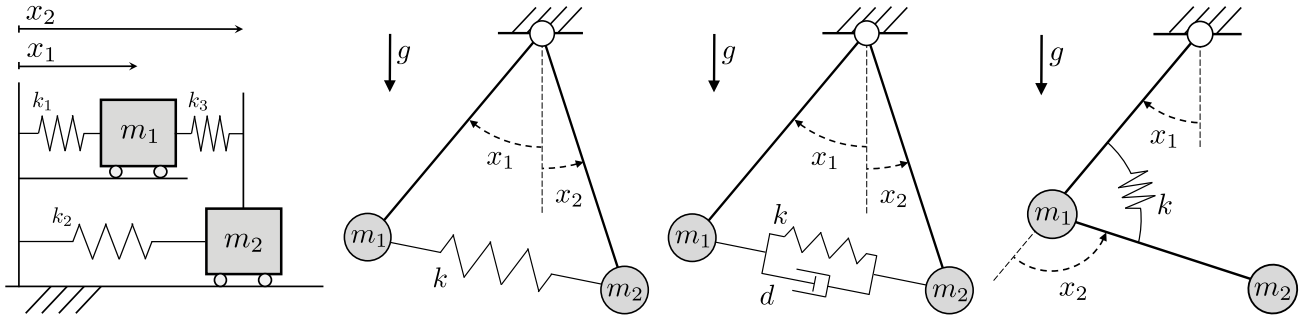

(a) Linear system (b) Nonlinear Euclidean system (c) Adding dissipation (d) Non-Euclidean system

Fig. 2. Mechanical systems with two degrees of freedom. Panel (a) shows a linear system. The two masses evolve along strict parallel lines, and they are connected by linear springs. Panels (b) and (c) depict mechanical systems with constant inertia tensor, but subject to a nonlinear potential field. The masses are connected at the tip of two pendulums, they are immersed in a gravity field, and a linear spring connects them. Note that for appropriate choice of parameters (a) matches to local behavior of (b). A dissipative element acts between the two masses in panel (c). Panel (d) shows a double pendulum. The same two masses are now inertially coupled. The inertia tensor is configuration dependent.

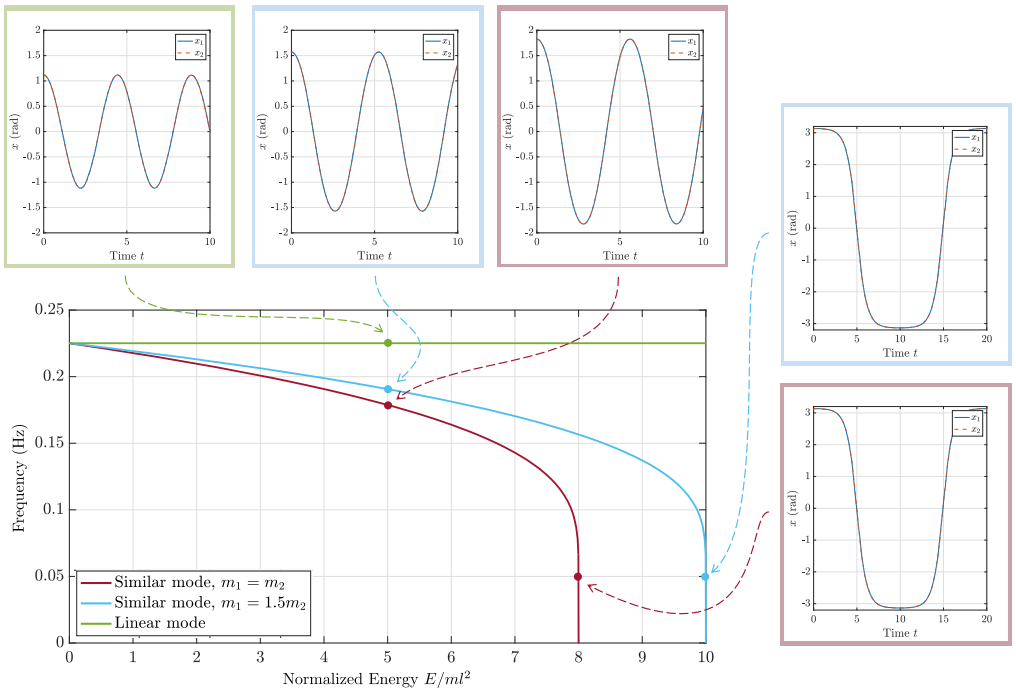

Fig. 3. In phase modes of the linear system (3), and the nonlinear system (19), shown by Fig. 2(a) and (b), respectively. The first system is the linearization of the latter, around the stable equilibrium. Both equal ($m_1 = m_2$) and different ($m_1 = 1.5m_2$) masses are considered. The energy-frequency plot is shown in the bottom left. The frequency of the linear system is constant. The frequencies of the nonlinear systems decrease with the energy increasing, and converges to 0 when the unstable equilibrium $x_i = \pm\pi/2$is reached. Examples of linear and nonlinear oscillations are shown for $E = 5ml^2$, and frequency $f = 0.05$Hz.

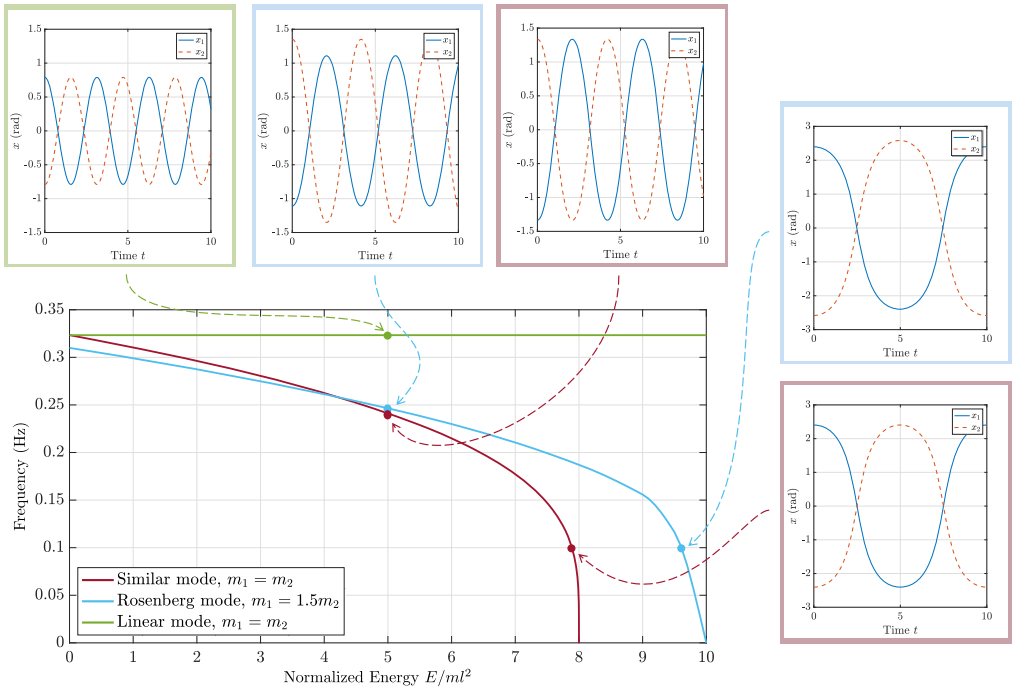

Fig. 4. Anti phase modes modes of the linear system (3), and the nonlinear system (19), shown by Fig. 2(a) and (b), respectively. The first system is the linearization of the latter, around the stable equilibrium, when $m_1 = m_2$. Both equal ($m_1 = m_2$) and different ($m_1 = 1.5m_2$) masses are considered. The energy-frequency plot is shown in the bottom left. The frequency of the linear system is constant. The frequencies of the nonlinear systems decrease with the energy increasing, and converges to 0 when the unstable equilibrium is reached (which is now different from $x_i = \pm\pi/2$). Examples of linear and nonlinear oscillations are shown for $E = 5ml^2$, and frequency $f = 0.05$Hz.

$$E(x,\dot{x}) = \frac{1}{2}\dot{x}^{\mathrm{T}}M(x)\dot{x} + V(x). \tag{7}$$

Eq. (6) is globally equivalent to (4), and (7) to (5), if $\mathcal{X} \simeq \mathbb{R}^n$. In this case $(\Phi, \mathrm{d}\Phi)$ can always be taken as to be a bijection.

3.1. Oscillations in weakly nonlinear systems

The mechanical system (6) is said to be weekly nonlinear if its dynamics can be rearranged as

$$\overline{M}\ddot{x} + Kx = \phi(x,\dot{x},\ddot{x},t), \tag{8}$$

where $\overline{M}$and K are some constant and positive defined matrices, and $\phi : \mathbb{R}^n \times \mathbb{R}^n \times \mathbb{R}^n \times \mathbb{R} \to \mathbb{R}^n$is small and/or simple, in some sense that needs to be specified case by case. A lot of attention has been dedicated to this class of systems over the years, since they have been regarded as a bridge between (1) and (6). It has for example been observed that they can present quite complex behaviors as bifurcations (Hill, Neild, & Cammarano, 2016a), chaos (Holmes, 1986), self synchronizations (Pikovsky, Kurths, Rosenblum, & Kurths, 2003), non trivial energy flows (Gendelman, Manevitch, Vakakis, & M'closkey, 2001).

The modes of the linearized system (discussed in Section 2) already give profound insights into the global behavior of weakly nonlinear

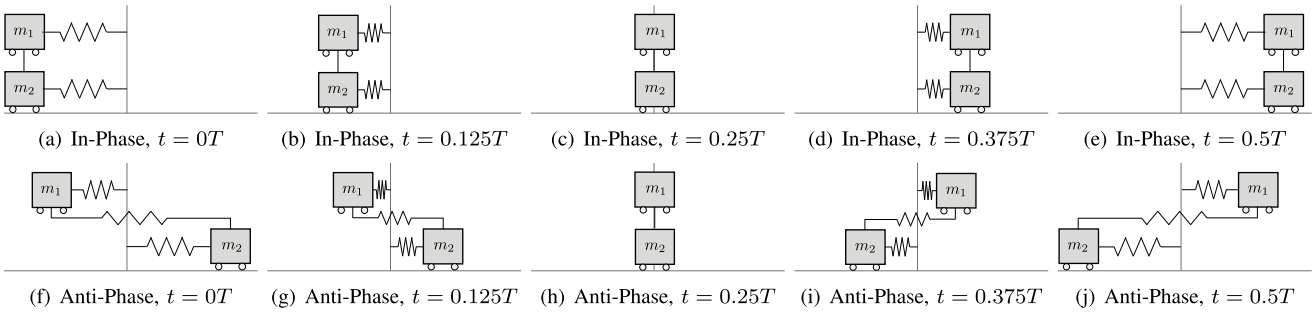

Fig. 5. Modal oscillations of the linear two mass system (see Fig. 2(a)), for $m_1 > m_2$. Panels (a–e) show half a period of an oscillation for the in phase mode. Panels (f–j) show half a period for the anti phase mode. The second part of the oscillations repeats backwards and it is therefore not shown.

systems (Hill, Neild, Cammarano, & Wagg, 2016b). This is nonetheless not sufficient in general. As an alternative, perturbation methods can be used when the weak nonlinearity must be directly taken into account. The key idea here is to express ϕ and x as a polynomial expansion w.r.t. a small real parameter ϵ, which can or cannot have some physical meaning. Then one can proceed by iteratively truncating the polynomials, solving the resulting problem, and substituting back the result. The method is detailed in Nayfeh (2008), and its use in control theory is surveyed by Kokotovic, Khali, and O'reilly (1999).

We will not discuss further the weakly nonlinear case here for two reasons. First, there are already several texts discussing the topic in detail (see references above). Second, and most important, reason is that the nonlinear mechanical systems we are practically interested into are strongly non linear.

3.2. Small oscillations in nonlinear mechanical systems

As a first step towards the full-fledged nonlinear case, we look at the behavior of (6) close enough to an equilibrium (i.e. low energies, small oscillations). It seems quite reasonable to expect to find at least n oscillations also in the nonlinear case. Indeed, a nonlinear system can always be locally approximated with its linearized version, which in turn in the generic case has n distinct oscillations for each energy level (as discussed in Section 2). Note, however, that having the linear evolutions approximating the nonlinear ones is not sufficient to assure periodicity. As a counterexample, consider that for any $\epsilon > 0$ we can always take an aperiodic function $\delta_x(t)$ such that $||\delta_x(t)|| < \epsilon$ for all t. Then, given a periodic trajectory of the linearized system $x(t)$, one can always build an aperiodic evolution which is in a ϵ neighborhood of $x(t)$ as $x(t) + \delta_x(t)$.

Despite not being thus a trivial consequence of linearization, the local existence of n periodic oscillations for the system (6) has been proven true by Horn (1903) in 1903, and by Lyapunov (1907) in 1907. Both proofs are given in the case of non resonant linearized system (i.e. the periods of the normal modes do not have integer ratios), and under the assumption that the Hessian of the system's energy is positive definite in the equilibrium (i.e. the energy is locally convex). The extension to the general case required more than sixty years, and it was finally provided by Weinstein (1973) in 1973, by relying on perturbation of periodic manifolds arguments. The result was further extended few years later to generic nonlinear systems in Moser (1976).

3.3. Large oscillations in nonlinear mechanical systems

Once n oscillations are established to exist for small amplitudes, the next natural step is to investigate if the same holds for higher energy levels. Intuition tells us that for continuity arguments this should be true under opportune regularity conditions. This is also backed up by some theoretical results, as for example early developments by (Poincaré, 1899) connecting small perturbations of the energy level to small variations of the orbit. The basic ideas for proving the existence of at least one periodic motion under particular conditions were introduced by Birkhoff (1917). Nonetheless, answering to the question more generally proven to be a quite complex challenge as well.

The main tools to address the existence and the number of different oscillations displayed by a nonlinear systems in mathematics and physics are differential geometry and algebraic topology as well as their application in Hamiltonian mechanics. The link between the dynamics of mechanical system and algebraic topology is given by the fact that the solutions of the conservative system (4) are geodesics in configuration space $\mathcal{X}$, with respect to the Jacobi metric

$$g_p = 2(\mathcal{E} - \mathcal{V}(p))\mathcal{I}_p, \tag{9}$$

where $\mathcal{I}_p$ is the inertia tensor. Therefore, all closed geodesics of g_p on $\mathcal{X}$ are periodic solutions of a mechanical system (4). A classical result, for example, states that, if $\mathcal{E} > \max(\mathcal{V}(p))$, then for every two integers n and m, there exists at least one periodic motion of the double pendulum from Fig. 2(d) making n rotations around the first joint and m rotations around the second joint. Such a trajectory is visualized in Fig. 7. The proof is based on the concept of equivalence classes of curves on manifolds (e.g. homology classes) and on the fact that within each such equivalence class the length of curves can be contracted until they become a geodesic (Arnold, 1989). The procedure leads to at least one geodesic in each equivalence class.

The periodic oscillations we are interested in as generalizations of single linear modes exhibit, however, some fundamental differences to the above periodic trajectories, which are closed curves. The modal oscillation, in contrast, have the topology of a line segment in configuration space. The segment is travelled back and forth during the oscillation, implying that the two ends of the segment are rest points. At these points velocity, and thus kinetic energy, are zero and therefore the Jacobi metric becomes singular. These kind of periodic oscillations are often called "breaking trajectories". Their treatment was first introduced by Seifert (1948). There, the existence of at least one closed orbit is proven for Hamiltonian systems with quadratic kinetic energy and potential V with level sets $\mathfrak{S}$ homeomorphic to a $n-1$ sphere (see Fig. 23 (c)). The trajectory is such that it begins and ends on the boundary of the maximum equipotential surface. The solution has been improved over the years to more general Hamiltonians. For example Rabinowitz (1977) proves the same thesis, under the milder hypothesis that the level sets of the energy are radially homeomorphic to a $2n-1$ sphere.

The original work by Seifert (1948) also introduced as a conjecture that - under the same set of hypotheses – the number of oscillations should actually be n for any energy level. The interest in this conjecture was revitalized in more recent times, see (Ekeland & Hofer, 1987; Gluck & Wolfgang, 1983). In the authors' best knowledge, as of today there is no general proof of this conjecture, this being still today a topic of active research, with increasingly general results (Giambó, Giannoni, & Piccione, 2020).

Yet, several weaker versions of the conjecture have been introduced and proven. in Gluck and Wolfgang (1983), the existence of n breaking trajectories is proven under certain non-resonance conditions. The paper

gives also a well readable overview on the earlier work. In the case of convex energy functions, Ekeland and Hofer (1987) proves that the number of oscillations for each energy level is always greater than one, as soon as $n > 1$. Note that an energy shell $\bigcup_{E<\bar{E}} \mathfrak{E}(E)$is always a convex set for convex energy functions (see Fig. 23(c)). The same result has been proven for star shaped energy surfaces under some non-degeneracy conditions (Hu & Long, 2002), and in a more general setting but with $n = 4$in Cristofaro-Gardiner, Hutchings et al. (2016). The conjecture is proven for $n = 3$in Wang, Hu, Long et al. (2007). The tightest lower bound for the general case of compact convex energy level is provided by Long and Zhu (2002), and it is equal to $\left\lfloor \frac{n}{2} \right\rfloor + 1$. The existence of $n$independent closed orbits has been proven for energy surfaces symmetric w.r.t. the origin Liu, Long, and Zhu (2002). Particularly relevant is the so-called pinched case introduced in Ekeland and Lasry (1980). Here, the conjecture is proven under the hypothesis that each energy level $\mathfrak{E}$is enclosed between two spheres, such that the larger has $\sqrt{2}$the radius of the smaller. Giambó et al. (2020) newly claimed the proof of a quite general case.

These results also suggest that in nonlinear systems, the number of oscillations can change with the energy level, and some of them can appear or disappear when energy increases. This can be observed in simulations and proven analytically for specific examples (we provide an example of this behavior in Section 8).

Also, it should be noted that nonlinear systems have a quite rich frequency palette when compared to linear systems. Rather than being constrained to n possible periods of oscillations (and their multiples), nonlinear mechanical system satisfying mild conditions on their energy function can be proven to have at least one orbit corresponding to all possible periods of oscillations (Benci, 1984; Rabinowitz, 1977).

Another last point is worth to be made here; in the practice of nonlinear mechanical systems with non constant inertia tensor, a very high number of periodic orbits exist for any given energy level. See for example bifurcation of limit cycles in Hamiltonian systems and Hilbert's sixteenth problem (Li, 2003, Section 2.5). This number can even grow to infinity, as noted in Ekeland and Hofer (1987). This can be intuitively explained by the dependency on configuration of the frequency of oscillation in nonlinear systems. This results in self-resonances that tend to increase in number with the energy. An example is shown by Fig. 6.

However, most of these oscillations will have a quite convoluted evolution, as also shown by the same figure. From a theoretical perspective this can be explained by considering that already in the two sphere S^2, the number of closed geodesics of maximum fixed length increases with the length at least as the prime numbers (Hingston, 1993). The results that we will discuss in the following aim at characterizing and collecting nonlinear oscillations which are *regular enough*, therefore investigating the intermediate parts of the spectrum in Fig. 1. See as example oscillation trajectories from Fig. 6 (e) and (p).

4. Rosenberg's nonlinear normal modes

The analyses discussed above lack of a fundamental ingredient of modal theory: grouping oscillations into similarity classes across energy levels. Closed orbits are indeed often studied as independent objects, and rarely connections are established explicitly between them. This classification is instead implicitly achieved in the linear case through the geometrical concept of eigenspaces ES_i (see Section 2). The first attempt to get back to this unifying view has been the concept of similar modes, that we discuss in the next subsection together with their generalization: the strict modes.

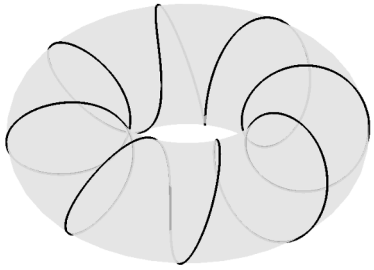

Fig. 7. Closed geodesics in configuration space with respect to the Jacobi metric of a mechanical system are closed periodic solutions of the system.

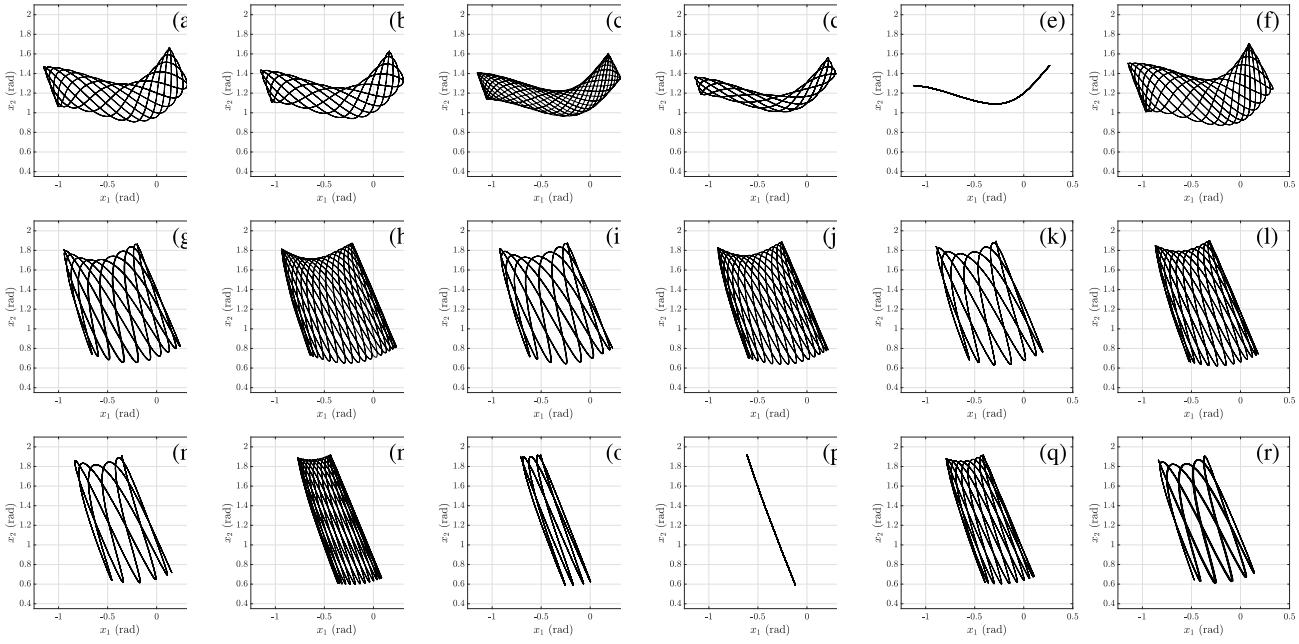

Fig. 6. Some examples of oscillations of a double pendulum with parallel elastic elements (see Fig. 2(d)). All evolutions are part of the same energy surface (2.5J), i.e. the initial conditions are part of $\mathcal{V}(p) = 2.5$J. The trajectories shown here are just few examples taken from the more than 40 periodic evolutions we could identify. Similar abundance of periodic orbits can be observed across energy levels, and for vast ranges of perturbations of the system parameters.

4.1. Similar and strict modes

Similar modes have been introduced by Rosenberg (1960), for nonlinear mechanical systems with Euclidean metric, i.e. with a constant inertia tensor. Therefore, $\mathcal{X} \simeq \mathbb{R}^n$, and the state is directly $(x, \dot{x})$. Their energy function (7)is speciliazed into

$$E(x,\dot{x}) = \frac{1}{2}\dot{x}^{\mathrm{T}} M \dot{x} + V(x). \tag{10}$$

This yields the following dynamics

$$M\ddot{x} + \frac{\partial V(x)}{\partial x} = 0, \tag{11}$$

with the inertia matrix $M \in \mathbb{R}^{n\times n}$being constant, positive definite, and diagonal, the latter without loss of generality. As in (6), the function $V : \mathbb{R}^n \to \mathbb{R}$is the system potential. It is considehere to be smooth, and convex. Eq. (11) models any finite set of discrete masses, coupled by means of possibly nonlinear potential fields. Examples are shown in Fig. 2(a) and (b).

Definition 2. (*Similar modes*) In analogy with standard linear modes, a periodic solution $x(t)$ of (11) is said to be a similar mode if it verifies

$$x(t) = c\, x_1(t), \tag{12}$$

for some $c \in \mathbb{R}^n$. These evolutions have a powerful property, making the subspace generated by c a proper generalization of eigenspaces: if (12) is verified by some $x(t)$, then it is verified by all the evolutions starting from an initial condition in Span{$(c, 0)$, $(0, c)$}. Therefore, c characterizes not just a single oscillation, but a whole family of them. The same is true in the linear case, where c is the corresponding eigenvector of $M^{-\frac{1}{2}} K M^{-\frac{1}{2}}$scaled such that its first component is 1. When trying to evaluate c for a nonlinear system, direct substitution in (11), and solution by inspection is typically the way to go. However, as it will appear clear soon, similar modes are the result of very particular symmetries of $V(x)$.

To better grasp the properties of similar modes, it is convenient examining first a more general case. Consider system (6), and the nonlinear generalization of (12)

$$x = X(x_1), \tag{13}$$

where $X : \mathbb{R} \to \mathbb{R}^n$. Again $x_1$is taken without loss of generality. This function allows to *bend* the straight eigenspace that we encounter in linear systems, transforming it into the following one-dimensional manifold in configuration space

$$\mathfrak{S} = \{x \in \mathbb{R}^n \,|\, x = X(x_1)\}. \tag{14}$$

According to the implicit function theorem this is a one dimensional submanifold of $\mathcal{X}$. Note indeed that the first element of $X$is the identity function, and therefore (13) effectively constraints $n - 1$degrees of freedom. In the following, we consider $\mathfrak{S}$to be connected. Note also that, since x_1 can be seen as a single parameter covering all $\mathfrak{S}$through the chart X, the manifold $\mathfrak{S}$must have the topology of a line. This excludes the other class of one dimensional manifolds, the ones homeomorphic to a circle S^1. Such a topology requires two charts to be completely covered, as shown in Fig. 21. This *bending* action effectively moves us a step to the right w.r.t. the linear (or similar) case in Fig. 1. Based on these considerations we can introduce the following concept, extending definition 2.

Definition 3. (*Strict modes*) Consider the case in which all $x(0) \in \mathfrak{S}$and $\dot{x}(0) \in T_{x(0)}\mathfrak{S}$are associated to an evolution $x(t)$ which is part of $\mathfrak{S}$for all $t > 0$. In this case we say that $x(t)$ is a strict mode.

This definition also implies that the associated tangent bundle $T\mathfrak{S} = \bigcup_{x\in\mathfrak{S}} \{x\} \times T_x\mathfrak{S}$is a two dimensional invariant manifold of the system.

One can now ask under which circumstances the conditions of Definition 3 are satisfied for some X. This question has been recently addressed by Albu-Schaeffer et al. (2019) (which actually tackles it in the general coordinate free setting). There, it is proven that the necessary and sufficient condition for this to happen is that the following two are simultaneously verified

i) at least a solution of (4) with $V \equiv 0$ satisfies (13),

ii) $\left(\frac{\partial^{\mathrm{T}} X}{\partial x_1}\frac{\partial X}{\partial x_1} I - \frac{\partial X}{\partial x_1}\frac{\partial^{\mathrm{T}} X}{\partial x_1}\right)\left(M^{-1}\frac{\partial V}{\partial x}\right)_{x=X(x_1)} = 0.$

The first condition is equivalent to asking that (13) identifies a geodesic of $\mathcal{X}$under the inertia tensor metrics. The second condition means that the accelerations due to the potential forces are tangent to X. Therefore, the inertia terms prescribe a library of possible candidates for X, which can then be either confirmed or discarded by the potential field.

Strict modes admit a natural extension to the dissipative case, as discussed in Calzolari, Della Santina, and Albu-Schäffer (2021). There, the condition of simultaneous diagonalization (introduced for linear systems in Section 2.2) is generalized by asking that dissipative action is always tangent to the potential force field.

System (11) has a constant inertia tensor (i.e. Euclidean metrics), which implies that the geodesics are all and only the straight lines. Therefore, the only $X(x_1)$ admitted in this case are the linear ones, i.e. similar modes are the only strict modes that can be observed in a system with constant inertia tensor. Vice versa, similar modes can appear in the general case (6), as discussed in Lakatos et al. (2017). Furthermore, condition (ii) gives an easy way to check whether a similar mode exists for (11). It is indeed sufficient to look for straight lines (geodesics of M in $\mathcal{X}$) along which the potential accelerations are aligned. An example will be provided in the next subsection.

Once the existence of a strict or similar mode is proven, one would like to extract a characterization of the behavior in time of the associated normal modes. This is unfortunately not possible to the extent we can get in the linear case, i.e. as analytic evolution of $x_1(t)$. However, we can write a one-dimensional dynamics which can later be integrated analytically or – more commonly – numerically. First, we derive twice (13)

$$\dot{x} = \frac{\partial X}{\partial x_1}\dot{x}_1, \quad \ddot{x} = \frac{\partial^2 X}{\partial x_1^2}\dot{x}_1^2 + \frac{\partial X}{\partial x_1}\ddot{x}_1. \tag{15}$$

These expression, are now substituted into (6). Some algebraic manipulations (including the pre-multiplication for $\partial^{\mathrm{T}} X/\partial x_1$) yield the one-dimensional mechanical system

$$M_{\mathrm{X}}(x_1)\ddot{x}_1 + C_{\mathrm{X}}\left(x_1, \dot{x}_1\right)\dot{x}_1 + G_{\mathrm{X}}(x_1) = 0, \tag{16}$$

with

$$M_{\mathrm{X}} = \frac{\partial^{\mathrm{T}} X}{\partial x_1} M(X) \frac{\partial X}{\partial x_1}, \qquad G_{\mathrm{X}} = \frac{\partial^{\mathrm{T}} X}{\partial x_1}\frac{\partial V}{\partial x}(X),$$
$$C_{\mathrm{X}} = \frac{\partial^{\mathrm{T}} X}{\partial x_1} C\left(X, \frac{\partial X}{\partial x_1}\dot{x}_1\right)\frac{\partial X}{\partial x_1} + \frac{\partial^{\mathrm{T}} X}{\partial x_1} M(X) \frac{\partial X^2}{\partial^2 x_1}\dot{x}_1,$$

where the argument of X is not shown for the sake of space. This can be strongly simplified in the similar case - i.e. when dealing with (11) and (12) – obtaining

$$M_{1,1}\ddot{x}_1 + \left(\frac{\partial V}{\partial x_1}\right)_{x=X(x_1)} = 0, \tag{17}$$

where $M_{1,1}$ is the element (1,1) of M.

Finally, note that (ii) is a rather strict condition, which cannot be expected to be fulfilled by arbitrary systems. It provides, however,

means to systematically design mechanical systems displaying strict modes. To cover the vast range of regular periodic behaviours encountered in the multi-body systems, not corresponding to strict modes, it is necessary to introduce a further generalization based on a relaxed set of conditions.

4.2. Example: two pendulums system

Consider the mechanical system depicted in Fig. 2(b). It is comprised of two pendulums, subjects to standard gravitational acceleration g, and connected with a linear spring with stiffness k. We consider them having same mass m and same length l. The state of the mechanical system is $(x_1, x_2, \dot{x}_1, \dot{x}_2)$. The total energy is

$$\begin{aligned} E\left(x_1, x_2, \dot{x}_1, \dot{x}_2\right) &= \frac{1}{2} ml^2 \left(\dot{x}_1^2 + \dot{x}_2^2\right) + V(x_1, x_2), \\ V(x_1, x_2) &= kl^2(1 - \cos(x_1 - x_2)) + mgl(2 - \cos(x_1) - \cos(x_1)). \end{aligned} \tag{18}$$

Standard derivations yield the following dynamics

$$\begin{bmatrix} \ddot{x}_1 \\ \ddot{x}_2 \end{bmatrix} + \frac{g}{l} \begin{bmatrix} \sin(x_1) \\ \sin(x_2) \end{bmatrix} + \frac{k}{m} \begin{bmatrix} \sin(x_1 - x_2) \\ \sin(x_2 - x_1) \end{bmatrix} = \begin{bmatrix} 0 \\ 0 \end{bmatrix}, \tag{19}$$

where we divided by ml^2 to get a more compact form. Note that the linearized system at the equilibrium state (0,0,0,0) is (3).

Fig. 8 (a) and (b) depict the potential acceleration field $-M^{-1}(x)V(x)$, for two choices of the system parameters. Applying condition (ii) of previous subsection (in this case the geodesics are strict lines), it appears clear that two similar modes exist. Confirming the prediction of the linearized system (see Section 2.1), one mode represents an in-phase oscillation, i.e. $c = (1, 1)$, and the other an anti-phase motion, i.e. $c = (1, -1)$. This can be verified by substituting $x_2 = \pm x_1$ into (19), and checking that the two equations become the same. The result is

$$\begin{aligned} x_1 &= +x_2 \Rightarrow \ddot{x}_1 + \frac{g}{l}\sin(x_1) = 0, \\ x_1 &= -x_2 \Rightarrow \ddot{x}_1 + \left[\frac{g}{l} + \frac{2k}{m}\cos(x_1)\right]\sin(x_1) = 0. \end{aligned} \tag{20}$$

Fig. 3 shows two energy-frequency characteristics of the in-phase mode, together with two examples of modal oscillations. The first one has energy equal to 5J, and its shape may recall the one of a simple cosine. However, its nonlinear nature is betrayed by the comparison with the oscillation of the linearized system, which is of higher frequency and lower amplitude. Note that such a change of frequency is a purely nonlinear behavior. The shape of the time evolution becomes clearly nonlinear for energies close to the maximum, approximating a rectangle wave. This is shown by the second example, in the right part of the same picture. The period of the wave gets longer and longer, until it gets to infinity (frequency equal to 0) - which condition corresponds to the unstable equilibrium of the pendulum. Fig. 3 reports similar results for the anti-phase mode. Fig. 9 depicts prototypical motions of the two pendulums, for both modes.

4.3. General Rosenberg's definition

The concept of modes of oscillation as an invariant set collecting trajectories of the same type is lost in the more general definition of Rosenberg's modes, which focus on a single oscillation. Indeed, Rosenberg defines in Rosenberg (1966) a nonlinear normal mode as an *oscillation in unison* of all masses, such that they all reach their peak and pass through the equilibrium configuration simultaneously. More specifically, the following definition holds.

Definition 4. (*Rosenberg mode*) A solution $\hat{x}(t)$ of (11) is said to be a nonlinear normal mode in the Rosenberg sense if

i) $\hat{x}(t)$ is periodic,
ii) a t^* exists such that $\hat{x}(t^*) = x_{eq}$,
iii) a $X : \mathbb{R} \to \mathbb{R}^n$ exists such that (13) is verified for $\hat{x}$,
iv) X is monotonic.

It is worth underlying that the strong difference between this definition and what we discussed in Section 4.1 lies in (iii). Whereas for similar and strict modes the existence of a single X was required for a continuous set of trajectories, here it is required to exist only for a single trajectory, and the focus is on a single energy level. Therefore, X does not identify the generalization of a whole eigenspace. On the contrary, it characterizes the geometry of a single, isolated modal evolution.

With the goal of evaluating $X(x_1)$, we differentiate (13) two times. The result is as in (15). Then, we use the closed form of the accelerations provided by (11), calculated in $x = X(x_1)$

$$-M^{-1}\frac{\partial V}{\partial x}(X) = \frac{\partial^2 X}{\partial x_1^2}\dot{x}_1^2 + \frac{\partial X}{\partial x_1}\left(-\frac{1}{m_1}\frac{\partial V}{\partial x_1}(X)\right). \tag{21}$$

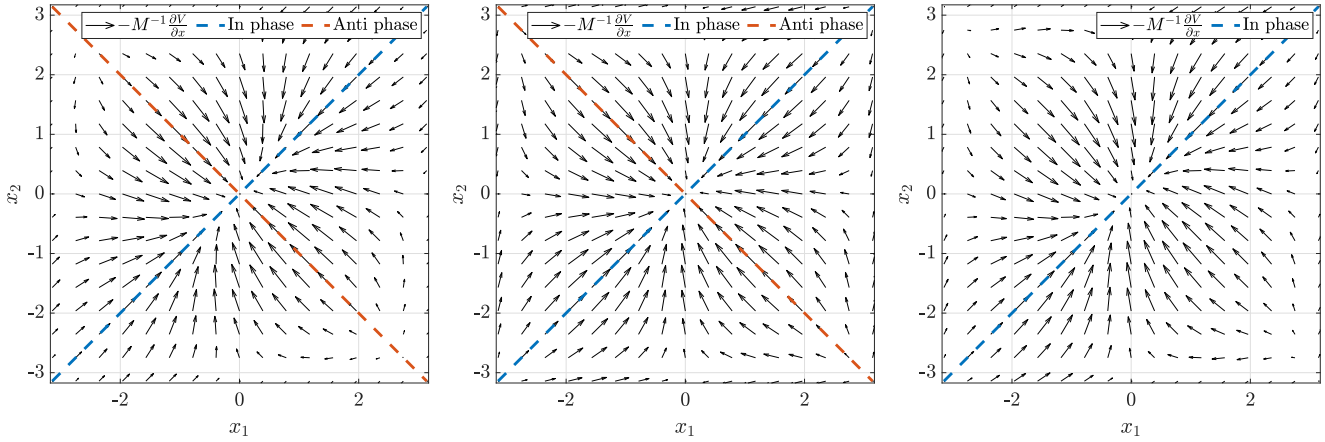

(a) $mg/kl = 2$, $m_1 = m_2$ (b) $mg/kl = 5$, $m_1 = m_2$ (c) $mg/kl = 2$, $m_1 = 1.5m_2$

Fig. 8. Potential acceleration field $M^{-1}\partial V/\partial x$ of the two coupled pendulums. Panels (a,b) show the case $m_1 = m_2$, for two choices of physical parameters. The field is always aligned along the two bisectors $x_1 = x_2$ and $x_1 = -x_2$. This suggests the presence of two similar modes, one in-phase and the other in anti-phase. Panel (c) report the different mass case $m_1 = 1.5m_2$. This change of mass distribution breaks the symmetry which produced the similar anti-phase mode - that becomes a standard Rosenberg modes (not shown in the picture). The in-phase mode is instead conserved.

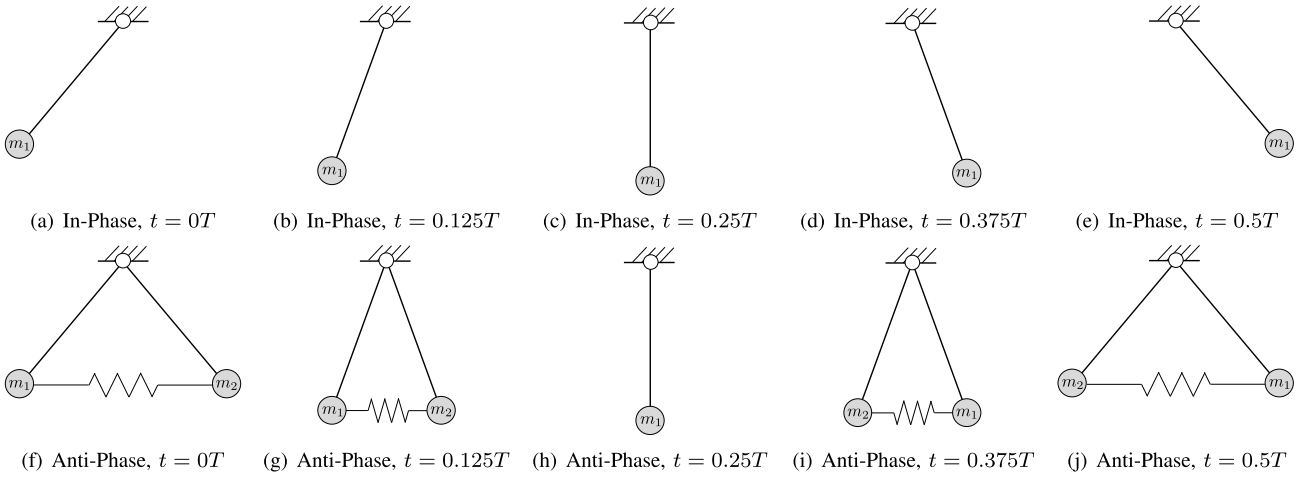

(a) In-Phase, $t = 0T$ (b) In-Phase, $t = 0.125T$ (c) In-Phase, $t = 0.25T$ (d) In-Phase, $t = 0.375T$ (e) In-Phase, $t = 0.5T$

(f) Anti-Phase, $t = 0T$ (g) Anti-Phase, $t = 0.125T$ (h) Anti-Phase, $t = 0.25T$ (i) Anti-Phase, $t = 0.375T$ (j) Anti-Phase, $t = 0.5T$

Fig. 9. Modal oscillations of the two pendulums system (see Fig. 2(b)), for $m_1 = m_2$. Panels (a–e) show half a period of an oscillation for the in phase mode. The two pendulums are here super-imposed, so only the first one is visible. Panels (f–j) show half a period for the anti phase mode. The second part of the oscillations repeats backwards and it is therefore not shown.

We now need to remove the explicit dependency on $\dot{x}_1$, since we aim at an X which is only configuration dependent. To this end, we exploit the fact that (11) is not subject to any dissipative force, i.e. the energy is constant along the evolutions. We call $\overline{E}$the constant energy level associated to $\widehat{x}(t)$. We combine (24)and (10), obtaining

$$\left(\frac{\partial^{\mathrm{T}} X}{\partial x_1} M \frac{\partial X}{\partial x_1}\right)\dot{x}_1^2 = 2\left(\overline{E} - V(X)\right). \tag{22}$$

We can now substitute back this expression in (21), with the following result

$$2\frac{\partial^2 X}{\partial x_1^2}\left(\overline{E} - V(X)\right) + \left(\frac{\partial^{\mathrm{T}} X}{\partial x_1} M \frac{\partial X}{\partial x_1}\right)\left(M^{-1}\frac{\partial V}{\partial x} - \frac{1}{m_1}\frac{\partial X}{\partial x_1}\frac{\partial V}{\partial x_1}\right) = 0. \tag{23}$$

The real solutions of this set of nonlinear partial differential equations characterize geometrically all the possible Rosenberg modes of (11), for the energy level $\overline{E}$.

As an alternative to solving (23) we can rely on continuation algorithms (Kvalheim & Bloch, 2019; Peeters, Viguié, Sérandour, Kerschen, & Golinval, 2009). The idea here is to proceed by direct integration of the dynamics, and optimize the initial condition for periodicity. The intersections of the eigenspaces of the linearized system with the energy level $\mathfrak{E}$are often used as starting point for these numerical methods. We will presentation an example of a continuation algorithm in Section 8.

4.4. Extended Rosenberg modes

Consider as a practically meaningful choice of x the positions of the oscillating masses measured from a fixed inertial frame. Expressed in these coordinates, Condition (iv) of Rosenberg modes asks that there is no time at which some of the masses reach their peak displacements, while others are still moving.

This excludes some oscillatory behaviors that we may want to consider in practice. For example, it is not possible for a mass to oscillate at twice the frequency of another mass. This condition is therefore often dropped in the practice, as discussed in (Kerschen et al., 2009, Sec 2.1). To stress the distinction between the two cases, we refer to these modes as Extended Rosenberg modes. As shown in Fig. 1, they represent another qualitative step in the direction of generic oscillations, moving farther away from the high regularity level of linear eigenmodes.

4.5. Rosenberg's manifold

Eq. (23) is clearly energy dependent, therefore we can expect to find different parametrizations of modal geometries for different energy levels. More specifically, the dependency on $\overline{E}$is smooth, and consequently we can expect the solutions X to change with a certain degree of continuity with respect to $\overline{E}$. Although overlooked or not clearly stated in the existing literature – this simple consideration allows to bring back the unifying view discussed above for strict modes, by explicitly collecting together related modes across energy levels. We refer to this family of solutions as

$$x = X\left(x_1, \overline{E}\right) \tag{24}$$

Note that this is not the same function as in (13) since here the energy is explicit as part of the domain. We are nonetheless using the same symbol for the sake of simplicity of notation. Such a parametrization can be attained as solution of (23), with the only formal difference that $\overline{E}$is now not just some fixed parameter but a variable itself.

We therefore propose to define an (extended) Rosenberg's manifold as a further geometrical generalization of the linear eigenspace, in the fashion of (14), as follows

$$\left\{(x, \dot{x}) \in \mathbb{R}^{2n} \,|\, x = X(x_1, E(x, \dot{x}))\right\}. \tag{25}$$

This is by construction an invariant sub-manifold of the state space $T\mathcal{X} \simeq \mathbb{R}^{2n}$. Note that a generic union of manifolds is not a manifold. Nonetheless, (25)defines a manifold thanks to the continuity of $\gamma_{(p,\ v)}(t)$ with respect all three arguments p, v, t, and also thanks to the uniqueness of the solution of the Cauchy problem - i.e. trajectories never intersect in the state space. Also, its dimension is 2, since it is built by merging a continuous set of one dimensional manifolds, parametrized with the one dimensional variable $\overline{E}$.

4.6. Example: two pendulums system with different masses

Consider now the two-pendulums system discussed in Section 4.2, when the two masses are not both equal to m but instead $m_1 = (1 + \delta)m$, and $m_2 = m$, with $\delta > -1$and $m > 0$.

It is immediate to see that the in-phase similar mode (i.e. $x_1 = x_2$) is maintained, for example by inspecting Fig. 8(c). This is a direct reflection of the well know isochronism of the pendulum.

In contrast, the anti-phase mode is perturbed, becoming a non-strict Rosenberg's mode. With the aim of characterizing its behavior, we

specialize (23) for the system under consideration

$$\frac{\partial^2 X_2}{\partial x_1^2}\frac{2\left(\overline{E}-V(X)\right)}{1+\delta+\frac{\partial X_2}{\partial x_1}}-\frac{1}{1+\delta}\frac{\partial X_2}{\partial x_1}\frac{\partial V}{\partial x_1}(X)-\frac{\partial V}{\partial x_2}(X)=0. \tag{26}$$

In the remaining part of the section we refer to left side of this equation as to $F(X,x_1,\overline{E})$.

Unfortunately, solving analytically (26) – and more generally (23) – is a virtually impossible task. As alternative, we can relax (23) in the Galerikin sense (Renson, Kerschen, & Cochelin, 2016), by considering an approximation for (24) in a finite dimensional sub-space of the solution space. A natural choice when X is supposed analytic are finite order polynomials

$$X\left(x_1,\overline{E}\right)=\sum_{i=1}^{m}c_i\left(\overline{E}\right)x_1^i+O\left(x_1^{m+1}\right), \tag{27}$$

where $c_i\in\mathbb{R}^n$are energy dependent gains, which generalize c in (12). So, this choice serves also as a direct extension to the similar case. Note that no constant term is present in X, since otherwise condition (ii) of Definition 4 could not be fulfilled. We can then perform a Taylor approximation of (23), to get a polynomial equation. The locally minimal error solution can the be found by selecting the c_i nullifying as many low order coefficients as possible of the resulting polynomial.

We consider here a third order approximation for the mode's parametrization

$$\tilde{X}\left(x_1,\overline{E}\right)=c_1\left(\overline{E}\right)x_1+c_2\left(\overline{E}\right)x_1^2+c_3\left(\overline{E}\right)x_1^3, \tag{28}$$

where c_i are scalar-valued functions. This function is then plugged into (26), and coefficients of a Taylor expansions around $x_1=0$are sequentially evaluated and imposed to be null. Although a solution can be computationally found for generic values of system parameters, we prefer to substitute here the values $k/m=1,g/l=2,\delta=1/2$,to show at least partially the derivations. The offset is $F(\tilde{X}(0),0,\overline{E})=4\overline{E}c_2$,which is zero only for $c_2=0$. The linear term of the expansion is

$$\left(\frac{\partial F}{\partial x_1}\left(\tilde{X}(0),0,\overline{E}\right)\right)_{c_2=0}=12\overline{E}c_3+\left({c_1}^2+\frac{3}{2}\right)\left(3c_1+\frac{2c_1(c_1-4)}{3}-1\right), \tag{29}$$

which we can nullify by taking c_3 as function of c_1. Interestingly, the quadratic term is already null thanks to the choice of c_2 that we already made. Finally, the coefficient c_1 can be evaluated as a solution of $\partial^2F/\partial x_1^3=0$. This expression is too long to be displayed. This provides two real solutions. The first one is $c_1=1$,which in turns implies $c_3=0$. This is the similar in-phase mode which we already predicted, and its characteristics are summarized by Fig. 3.

A second solution is also present, and it represents the anti-phase nonlinear mode. Unfortunately, also this solution is too long to be displayed. We instead resort to plotting the corresponding behavior. Fig. 10 (a) depicts five examples of anti-phase nonlinear modes, associated to different energy levels. Both simulation results, and values predicted by the third order approximation are shown. With the increase in energy the oscillations of the lighter pendulum tend to decrease, approaching in amplitude the ones of the heavier weight.

We also report the energy-frequency characteristics of the mode in Fig. 4, together with two examples of modal oscillations. The frequency of oscillation follows a similar trend as for the similar case, shown in the same picture. One of the two examples is for $\overline{E}=5$J. In this case $\tilde{X}(x_1,5)\simeq 0.019x_1^3-1.3x_1$. Finally, the Rosenberg's manifold is reported in Fig. 10(b) and (c), through two projections.

5. Shaw-Pierre's nonlinear normal modes

The focus of this paper is on conservative systems. Nonetheless, we take here a brief detour to the variable-energy case to discuss Shaw-Pierre nonlinear normal modes (see Fig. 1). We decided to discuss them in this paper for two reasons. First, they are a so popular concept in nonlinear modal theory, that they cannot miss in a survey on the topic. Second, the idea of applying a geometric view to the problem was originated by this sub-field of modal theory - as we will clarify later in this section.

5.1. Definition

Consider the dissipative systems with Euclidean metrics

$$M\ddot{x}+\frac{\partial V}{\partial x}=-D(x)\dot{x}, \tag{30}$$

where $D:\mathbb{R}^n\rightarrow\mathbb{R}^{n\times n}$is a (semi-)positive definite matrix valued function, modelling the mechanism damping. As a result of damping actions, the energy of the system is no more constant, but decreases with time

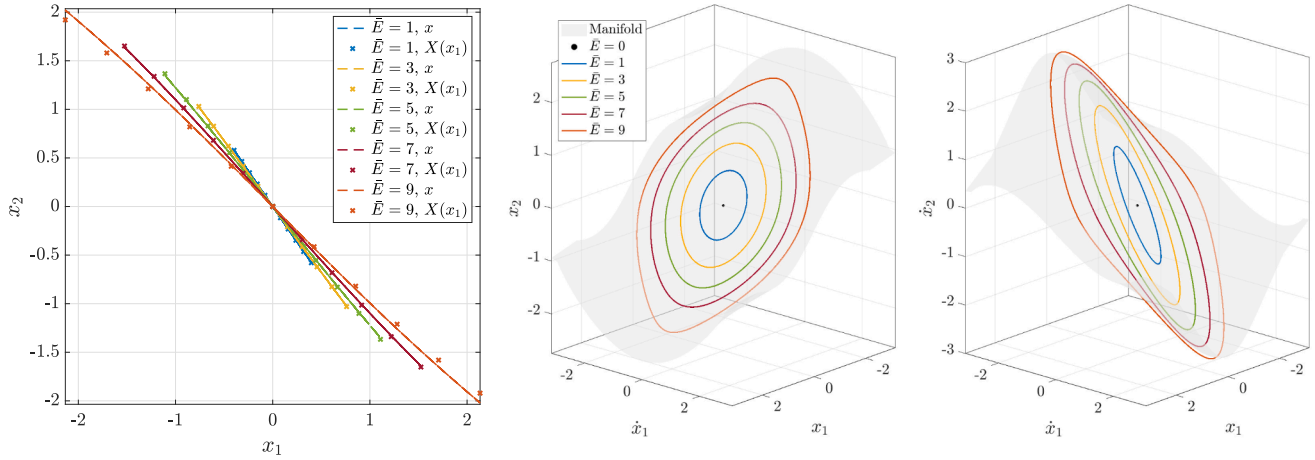

(a) Evolutions (b) Manifold, Projection 1 (c) Manifold, Projection 2

Fig. 10. Non-similar Rosenberg mode of the to two pendulums system with $m_1=1.5m_2$. This is the extension of the linear anti-phase mode. With the increase of $m_1$the similar mode ($x_1=-x_2$) bends into a more general Rosenberg mode. Panel (a) shows five instances of the mode, for various energy levels. Values predicted by (28)are also shown. The associated Rosenberg's manifold is shown in panels (b,c). Since the state space is of dimension four, we look at the sub-manifold through two projections: in Panel (a) to $(x_1,\dot{x}_1,x_2)$, in Panel (b) to $(x_1,\dot{x}_1,\dot{x}_2)$. The same five modal evolutions are also shown, together with the equilibrium.

$$\dot{E} = -\dot{x}^{\mathrm{T}} D(x)\dot{x} \leq 0. \tag{31}$$

Any mechanical system that can be modelled through (10) falls into this class when any form of smooth dissipation is added. Fig. 2(c) shows an example of such a system. Note that the inertia tensor is here still constant. in Shaw and Pierre (1993), Shaw and Pierre proposed an extension of linear modes to this class of dissipative systems, as follows

Definition 5. (*Shaw-Pierre mode*) A two dimensional sub-manifold of the state space is a Shaw-Pierre modal manifold of (30) if

i) it is invariant,
ii) it is tangent to an eigenspace *ES* of the linearized system at the equilibrium.

Any evolution $x(t)$ contained in the modal manifold is said to be a nonlinear normal mode in the Shaw-Pierre sense.

These are characteristics which are implicit in the definition of Rosenberg manifold (see Section 4.5). A nonlinear mode is any evolution of the system contained in this invariant manifold.

As a direct extension of linear eigenspaces (see Section 2.2), Shaw-Pierre modes can be effectively used for model reduction of high dimensional systems (Shaw & Pierre, 1994).

Although this does not strictly appear as part of the of the definition, later in the text the authors ask that two functions $X, \dot{X} : \mathbb{R}^2 \to \mathbb{R}^2$ exist such that the following equations hold on the manifold

$$x = X\left(x_1, \dot{x}_1\right), \quad \dot{x} = \dot{X}\left(x_1, \dot{x}_1\right), \tag{32}$$

where, as in (13) and (24), x_1 and $\dot{x}_1$ are taken without loss of generality. In turn, (32) allows to define the Shaw Pierre manifold in analogy to the strict and Rosenberg's ones - Eqs. (14) and (25) respectively - as follows

$$\left\{(x, \dot{x}) \in \mathbb{R}^{2n} \mid (x, \dot{x}) = \left(X\left(x_1, \dot{x}_1\right), \dot{X}\left(x_1, \dot{x}_1\right)\right)\right\}. \tag{33}$$

Again, this is a two dimensional submanifold of $T\mathcal{X} \simeq \mathbb{R}^{2n}$ due to the implicit function theorem.

It is important to stress that although our treatise of the topic aims at proposing an unifying view trough a geometric formalism, the use of manifolds to describe modes was first established by the efforts of Shaw and Pierre (1993), who in turn took inspiration from central manifold theory (Guckenheimer & Holmes, 2013, Section 3.2).

5.2. Indeterminateness of the definition and its resolution

Given a Shaw-Pierre manifold, we can build possibly infinite many others. This can be done by deforming with continuity the original manifold everywhere outside a neighborhood of the equilibrium, and in such a way that condition (i) is fulfilled. This makes this concept well defined only locally. Similar issues with Shaw-Pierre definition have been pointed out in recent years by multiple authors, see for example (Haller & Ponsioen, 2016; Neild, Champneys, Wagg, Hill, & Cammarano, 2015).

These considerations are however largely overlooked, since the original paper (Shaw & Pierre, 1993) already introduces a way of implicitly solving this redundancy. This is done by specifying a method to approximate $X, \dot{X}$ as the fix order polynomial functions that are closest to verifying conditions (i) and (ii). In this way a single manifold is unequivocally selected among all the possible candidates.

This strategy works well in the practice, allowing to study continuations of linear modes in a neighborhood of the equilibrium. On the downside, it induces the insidious weak point that different ways of evaluating Shaw-Pierre manifolds de facto introduce different definitions of the concept (Cirillo, Mauroy, Renson, Kerschen, & Sepulchre, 2016; Pesheck, Pierre, & Shaw, 2002).

5.3. Forced oscillations

An interesting feature of Shaw-Pierre analysis is the ability of naturally taking into account forced systems. The key idea here is to add an exogenous system that keeps track of the passage of time

$$\dot{\tau} = \omega_{\mathrm{F}}, \quad M\ddot{x} + \frac{\partial V}{\partial x} = -D\dot{x} + F(\tau), \tag{34}$$

where $\tau \in \mathbb{R}$ is a scaled time variable, $\omega_{\mathrm{F}} \in \mathbb{R}$ is the frequency of oscillation, and $F : \mathbb{R} \to \mathbb{R}^n$ defines the pattern of oscillation. In this context, the dimension of the modal manifold is typically increased to three, and τ is added along x_1 and $\dot{x}_1$ as a parameter - i.e. the manifold structure is effectively time variant. Sinusoidal excitations are considered in Jiang, Pierre, and Shaw (2005), while the general case is tackled in Gabale and Sinha (2011).

Of note, we should also underline that this is not the only strategy to study nonlinear modes in dissipative and forced systems. A common alternative is looking at the modes of the underlying conservative autonomous system, which can be shown to define the resonance peak backbone of the non conservative case (Hill et al., 2016a; Hong, Hill, & Neild, 2019).

6. Other definitions

Rosenberg's and Shaw-Pierre's definitions are by far the two most successful and accepted extensions of modes to the nonlinear case. However, other definitions exist, being deeply interesting in their own regards. We present in the following a selection of them, without any claim of exhaustiveness.

6.1. Spectral manifolds

Spectral manifolds (Haller & Ponsioen, 2016) are defined as the smoothest invariant manifold tangent to a spectral subbundle along an evolution composed of finitely many frequencies - which is called nonlinear normal mode in this context. Therefore, rather than a collection of modes, the spectral manifold is a way of describing a low dimensional section of the basin of attraction of a single regular evolution. Also note that the nonlinear mode so defined is a weaker concept than the general oscillation in Fig. 1. In case an equilibrium is considered as reference evolution, the associated spectral subbundle is an eigenspace of the linearized system. In this case, the spectral manifold defines a way of resolving the indeterminateness discussed in Section 5.2, by selecting the smoothest Shaw Pierre invariant manifold.

Spectral manifolds for non-conservative mechanical systems with constant inertia tensors are studied in Haller and Ponsioen (2016), and conditions for existence and uniqueness are provided. An example of application to a two degrees of freedom system with variable inertia is provided in Szalai, Ehrhardt, and Haller (2017).

6.2. Koopman operator

Linear modes can be extended in a way that maintains the superposition effect, by means of the Koopman operator. Consider the Hilbert space of all the possible measures that can be taken from a nonlinear dynamical system (i.e. all the possible functions of the state). In his 1931 paper (Koopman, 1931), Koopman proved that the original nonlinear dynamics always becomes linear - although infinite dimensional - when expressed in this functional space. The operator describing the update function of this linear dynamics is called Koopman operator.

The key idea now is to compute the eigenspaces of the linear system by spectral analysis of the Koopman operator - and possibly map them back to the original space (Mezić, 2005). In this way the invariance is

inherited by the invariance of the eigenspace. Additionally, the standard sum in the infinite dimensional space induces a way of combining modal evolutions so to recover modal superimposition.

However, the sets so constructed do not necessarily capture any salient regularity of the original system (for example the evolutions are not periodic). Moreover, they are infinite in number, ending up covering the large part of the configuration space. The latter issue is addressed by considering finite dimensional and possibly data-driven approximations of the linear system (Williams, Kevrekidis, & Rowley, 2015).

Another interesting use of the Koopman operator in modal theory has been proposed by Cirillo et al. (2016). There, authors prove that a Shaw-Pierre manifold can always be selected as the zero level set of select eigenfunctions of the operator.

6.3. Nonlinear eigenvectors

The control community has produced over the years several extensions of Eigenvalues and Eigenvectors to the nonlinear case. These are not explicitly related to the concept of modes, but still they are worth mentioning in this context due to the discussed connection between modes and spectral decomposition in linear systems. All these techniques are also not explicitly developed for mechanical system, but for generic nonlinear and smooth systems instead. in Padoan and Astolfi (2019), $f--$ reducing manifolds are introduced as an extension to the nonlinear domain of $A--$ reducing pairs. The latter in turn are a slightly more general concept than eigenspaces. Eigenvalues are then defined as specific vector fields on the $f--$ reducing manifold. These mathematical objects are then used to perform model reduction. in Halás and Moog (2013), an alternative definition of eigenvalues and eigenvectors is introduced, as the solution of a differential eigenvalue problem

$$A(x,\dot{x})e(x,\dot{x}) = \dot{e}(x,\dot{x}) + \lambda(x,\dot{x})e(x,\dot{x}), \tag{35}$$

with A being the Jacobian of the dynamical system, and e and λ being the eigenvector and the eigenvalue respectively. in Kawano and Ohtsuka (2015) diagonalizability of a nonlinear system is defined as the possibility of transforming the system into n one-dimensional subsystems. Then, necessary and sufficient conditions for diagonalizability are given in terms of the Einvectors as defined above. This result is combined with contraction analysis in Kawano and Ohtsuka (2017).

7. Nonlinear modes of a multi-body system

The aim of this section is making a further step towards generality of the notion, by establishing a new concept of nonlinear modes for mechanical systems with non constant inertia tensor. In analogy to what we discussed in Sections 4 and 5 for narrower classes of mechanical systems, our goal here is identifying a description of periodic trajectories that are the continuation of the linearized modes. We want them to be general but also specific enough to expect to find n modes for a system with n degrees of freedom as for the linear case, and corresponding to the Seifert conjecture discuss in Section 3.

Reaching this goal implies taking two steps: (i) assessing which parts of Rosenberg mode definitions can and cannot be directly retained in this context; (ii) introducing a definition of modes which can be applied to (4).

7.1. The need for relaxing Rosenberg's mode definitions

Consider Rosenberg modes as detailed in Definition 4, Sections 4.3 and 4.4. Ideally, we would like to maintain as many conditions as possible from it, to characterize the most regular evolutions of the system (4).

As we already discussed in Section 3, we can expect to have many closed orbits under mild assumptions on the potential field $\mathcal{V}$. Some of them will have a segment topology in configurations space, others a S^1topology, and other will self intersect. Fig. 6 shows some of the many periodic trajectories that we can find already in a double pendulum, for a fixed energy level. So solely periodicity as a requirement seems not to restrict enough the trajectories we are searching for.

The same analysis suggests that we can find trajectories that can be parametrized with a single variable - i.e. line-shaped and not self intersecting (see Fig. 6 (e,p)). We will therefore keep conditions (i) and (iii) of Definition 4 in place. Our investigations performed in simulations, suggest that at least 2 of these evolutions always exist for system evolving in a configuration space $\mathcal{X}$of dimension 2. The same seems to appear for $n = 3$, as we discuss in Della Santina and Albu-Schäffer (2020). However, providing a formal existence result is not a trivial matter, and it will require thoughtful analysis in future work.

We must, however, drop condition (ii). This is because oscillations in non Euclidean systems only rarely pass through the equilibrium. This can be clearly understood by looking at the problem represented in coordinates. The instantaneous acceleration of system (11) is always zero when passing through an equilibrium. This is not the case for system (6), where Coriolis and centrifugal forces introduce a dependency on $\dot{x}$which in general does not vanish when $x = x_{\text{eq}}$and $\dot{x} \neq 0$- even if examples can still be identified where this happens due to particular symmetries in the metric tensor. We can therefore expect the configuration with peak velocity to move far away from the equilibrium configuration with the increase of energy - towards close regions in $\mathcal{X}$where the potential field is locally aligned with the instantaneous acceleration due to inertia terms. Therefore, leaving condition (ii) in place would mean excluding the vast majority of periodic behaviors that (4) can produce. Instead, we will introduce in the next sections a weaker form of connection to the equilibrium through geometric arguments. Finally, we already motivated the relaxation of condition (iv) of Definition 4 in Section 4.4. For the same reasons, we will not consider this property here neither.

We are therefore moving a step further towards the right side of the spectrum laid down in Fig. 1.

7.2. Generator

As we already observed in Sections 4.5 and 5.1, while moving from the linear to the nonlinear realm, the eigenspace (2-dimensional subspace of $T\mathcal{X} \simeq \mathbb{R}^{2n}$) bends into a sub-manifold of the tangent bundle. Here we lay down the ground for providing a coordinate independent definition of the modal manifold, working in the general Riemann metric case. We do that by introducing an intermediate geometrical concept that will later be used for both theoretical definition and computations: the generator $\mathfrak{R}$. Fig. 11(a) shows an example of a generator, with main ingredients highlighted. See Fig. 23and appendix section for more details on the notation. In particular, the operator G evaluates the forwards and backwards evolution of system (4), and $\partial\mathfrak{R}$is the boundary of $\mathfrak{R}$.

Definition 6. (*Generator*) Consider a 1-dimensional connected submanifold $\mathfrak{R}\subseteq T\mathcal{X}$. We call it a generator for $\mathfrak{M}$if

i) $\mathfrak{M} = G(\mathfrak{R})$is a 2-dimensional (invariant) manifold,
ii) $\forall (p,v) \in \mathfrak{R}$, then $v = 0$,
iii) $(p_{\text{eq}}, 0) \in \partial\mathfrak{R}$exists such that $\{(p_{\text{eq}}, 0)\}$ is invariant - i.e. it is an equilibrium; no other point in $\mathfrak{R}$fulfills the same condition.

If a $2--$ dimensional manifold $\mathfrak{M}$admits a generator $\mathfrak{R}$, then it can be seen as a collection of evolutions of increasing energy starting from a local minimum (see Fig. 11(a)). Then, according to this definition, $\mathfrak{R}$collects one of the resting points of each trajectory in $\mathfrak{M}$. More formally, the manifold has a fiber bundle structure, with $\mathfrak{R}$being the base space, and the trajectories being the fibers. In case the trajectories are oscillations (breaking trajectories), there are two resting points from which we can equivalently pick. It is worth stressing once more that not

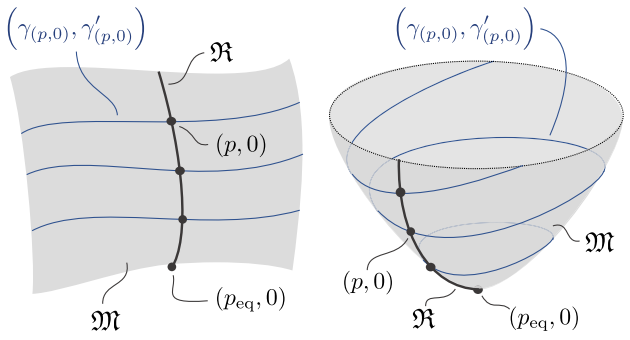

(a) Generator (b) Eigenmanifold

Fig. 11. Panel (a) shows the generator idea. $\mathfrak{M}\subset T\mathfrak{X}$is a two dimensional invariant manifold. It is constructed by applying the operator G to the generator $\mathfrak{R}$, which is a collection of points in $T\mathfrak{X}$with zero velocity. To each point $(p, 0) \in \mathfrak{R}$a different trajectory $(\gamma_{(p,v)}, \gamma'_{(p,v)})$is associated. This gives to $\mathfrak{M}$a fiber bundle structure, with base space $\mathfrak{R}$. If the trajectories collected in $\mathfrak{M}$are periodic (closed orbits) then $\mathfrak{M}$assumes the shape shown in panel (b). This is an eigenmanifold if $\pi_{\mathfrak{X}}\circ G(\{(p, v)\})$are line shaped (not shown in figure).

all the collections of one dimensional manifolds are manifolds themselves, and that this is the case here thanks to the continuity of $\gamma_{(p,0)}(t)$ with respect to all the arguments, and to the uniqueness of the solutions of the Cauchy problem.

The one dimensional manifold $\mathfrak{R}$has the role of a collector of labels for these trajectories. In turn, these labels can be expressed as a value in $\mathbb{R}$by finding a global chart for the generator. The energy is a good candidate for this role, defined as

$$\mathcal{E}\circ\Sigma_{\mathfrak{R}} : \mathfrak{R}\rightarrow\mathbb{R}, \tag{36}$$

where $\mathcal{E}$is the energy function defined in $T\mathfrak{X}$, and $\Sigma_{\mathfrak{R}}$is the natural embedding of $\mathfrak{R}$in $T\mathfrak{X}$. Note indeed that $\mathcal{E}\circ\Sigma_{\mathfrak{R}}$extracts the potential energy $(p, 0)\mapsto\mathcal{V}(p)$, which is monotonic if we consider the ordering of $\mathfrak{R}$induced by the metric tensor in $\mathfrak{X}$. Indeed, a critical point would be a second equilibrium, which is excluded by hypothesis (iii) of Definition 6. It is therefore a continuous injection, and it can be used as a global chart for $\mathfrak{R}$. This also implies that the generator must always have a segment topology.

7.3. Eigenmanifold

Now, that we have selected the type of trajectories that we wish to call modes in Section 7.1, and we introduced the necessary geometrical preliminaries in Section 7.2, we can merge them to propose a general definition of nonlinear normal modes and Eigenmanifolds for (4). Fig. 11(b) shows the main ingredients used in the definition.

Definition 7. (*Eigenmanifold*) A 2-dimensional sub-manifold $\mathfrak{M}\subset T\mathfrak{X}$admitting a generator $\mathfrak{R}$is an Eigenmanifold if all evolutions $\gamma_{(p, v)}$ contained in it are periodic and line-shaped, i.e.

i) **Periodic:**
$T : \mathfrak{R}\rightarrow\mathbb{R}^+$exists such that $\gamma_{(p, v)}$ is $T_{(p,v)}-$ − periodic,

ii) **Line-shaped:**
$O_{(p,v)} : \pi_{\mathfrak{X}}\circ G(\{(p, 0)\})\rightarrow[0, 1]$exists continuous with continuous inverse, $\forall(p, 0) \in \mathfrak{R}$such that $\mathcal{E}\circ\Sigma_{\mathfrak{R}}(p, 0) < \infty$,

If this is the case, we say that $\gamma_{(p, v)}$ is a nonlinear mode.

An Eigenmanifold is therefore defined as a manifold having a generator, and at the same time collecting trajectories verifying the two conditions introduced in Section 7.1. Indeed, (i) and (ii) in Definition 7 are the coordinate free expressions of (i) and (iii) in Section 4.3. The first condition is a direct counterpart of the original one. The second condition asks that every trajectory of the system (i.e. the image of the evolution $G(\{(p, 0)\})$ projected on $\mathfrak{X}$through $\pi_{\mathfrak{X}}$) is homeomorphic to a line. Note that the line is the only 1-dimensional manifold which can be globally parametrized through a single variable and a single chart – which is what condition (iii) in Definition 4is asking. This excludes evolutions of the kind shown in Fig. 12(a) – which is not a simple curve (i.e. it self-intersects) – as well as the one in Fig. 12(b) – which has S^1 topology. Looked from the lenses of Rosenberg's definition, both trajectories would need at leas two variables to be globally parametrized.

Finally, note that by collecting all the evolutions we further reduce the set of admitted oscillations. In this way we partially reintroduce condition (ii) of Rosenberg (Definition 4). Rather than asking that all the trajectories are directly connected to the equilibrium (which is not feasible as discussed in Section 7.1), we ask instead that they are parts of a single geometrical structure, which in turns contains the equilibrium point. We basically ask that the modes continuously *grow* from the equilibrium and an associated linear mode. Therefore, isolated line-shaped and periodic orbits which may appear and disappear with the increase of energy are not modes according to our definition. We instead take into account only oscillations that are already present arbitrarily close to the equilibrium point, where they can be approximated by - and therefore connected to - the modes of the linearized system. We consider this to be the main argument in favour to the proposed geometrical view to the problem.

7.4. Conceptual examples

We cannot provide yet an actual example showing the application of the proposed concepts. To get there, we must first introduce ways of calculating a representation of $\mathfrak{M}$for a given mechanical system. We will introduce such a method in the next section, where we also provide a full characterization of the nonlinear modes of oscillation for a double pendulum with parallel elasticity (as the one in Fig. 2(d)). We should however notice that in its core ideas this definition is quite akin to the manifold (25) generated by Rosenberg's modes, which can therefore be taken as a mental reference until the next example. The next subsection should help to further clarify this connection. Also, we sketch a representative set of modes in Fig. 13. We show here how a collection of modes would look like in terms of configuration coordinates, which is how we will often look at them in practice. The map $\Phi\circ\pi_{\mathfrak{X}}$implements the transformation from $T\mathfrak{X}$to $\mathbb{R}^n$. The natural embeddings are omitted for the sake of space. Among the other things, the picture clearly shows that the existence of a generator $\mathfrak{R}$serves as an extension of condition (ii) of Definition 4, by connecting each mode to the equilibrium x_{eq}.

7.5. Tighter definitions

We conclude this section by connecting our definition of an Eigenmanifold with the other extensions to the conservative case discussed in the first part of this paper. This is done by introducing subclasses of Definition 7, providing coordinate free counterparts of the already

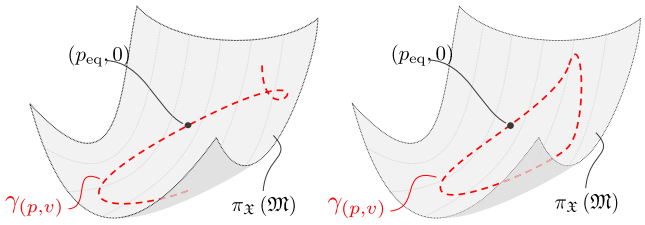

(a) Self-intersecting (b) S^1 topology

Fig. 12. Examples of oscillations which are not modes according to our definition, since they do not fulfill condition (ii) in definition 7 - i.e. they are not line shaped. Note that $\pi_{\mathfrak{X}}(\mathfrak{M})$is the projection of $\mathfrak{M}$in the configuration space $\mathfrak{X}$.

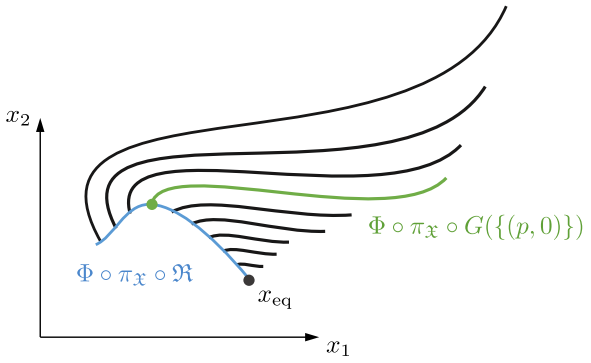

Fig. 13. A collection of nonlinear modes associated to a same eigenmanifold $G(\mathfrak{R})$when looked in configuration coordinates. Note that $\Phi \circ \pi_{\mathfrak{X}}$projects first in configuration space $\mathfrak{X}$and then expresses the configuration in coordinates. The generator $\mathfrak{R}$is shown in the picture as a light blue line. The other end of the oscillaitons could have been equivalently picked as the generator of the eigenmanifold. The trajectory of a single exemplary mode is highlighted in light green. Its starting point $(p, 0) \in \mathbb{R}$is depicted with a green circle. (For interpretation of the references to color in this figure legend, the reader is referred to the web version of this article.)

introduced manifolds.

Definition 8. (*Extended Rosenberg Mode*) An Eigenmanifold $\mathfrak{M} = G(\mathfrak{R})$is a Rosenberg manifold if $p_{\text{eq}} \in \pi_{\mathfrak{X}} \circ G(\{(p,v)\}), \forall (p,v) \in \mathfrak{R}$. If this is the case, we say that $\gamma_{(p,\, v)}$is a nonlinear mode in the Extended Rosenberg sense.

Definition 9. (*Strict Mode*) An Eigenmanifold $\mathfrak{M}$is strict if $\pi_{\mathfrak{X}}(\mathfrak{M})$can be given the structure of a one dimensional manifold. If this is the case, we say that $\gamma_{(p,\, v)}$ is a strict mode.

8. Methods: identification of modes

Definitions 6 and 7 allow for easily building a numerical representation of the Eigenmanifold, and for deriving simple methods for computing it. The algorithms that we will propose fall into the class of continuation methods. We refer to Peeters et al. (2009) and Kvalheim and Bloch (2019) for more details on the topic.

8.1. Connecting different energy levels

A main characteristics of Definition 7 is to group similar oscillations with increasing energy. We propose here a general way of connecting different energy levels, in a manner that is meaningful in the context of modal analysis. This is a necessary step to get to the computational aspects in the next subsections.

To this end, we assume that all equipotential energy levels $\mathfrak{E}_{\bar{E}} \subset \mathfrak{X}$(see Fig. 23(c)) are diffeomorphic to the $(n-1)$-dimensional sphere, through

$$\mu_{\bar{E}} : \mathfrak{E}_{\bar{E}} \to S^{n-1}. \tag{37}$$

This is an hypothesis that we already encountered in Section 3.3. We will use this mapping to connect all energy levels by projecting all of them on a same lower dimensional structure. For example, $\mu_{\bar{E}_2}^{-1} \circ \mu_{\bar{E}_1}$ can be used to map points from $\mathfrak{E}_{\bar{E}_1}$ to $\mathfrak{E}_{\bar{E}_2}$. We also further consider $S^{n-1}$to be equipped with a metric, which induces through μ a concept of closeness among points in $\mathfrak{X}$which is energy-invariant. Fig. 14 provides a visual intuition on this machinery.

One simple way of implementing μ in a neighborhood of the equilibrium is to use the chart Φ to map $\mathfrak{E}_{\bar{E}}$into $\mathbb{R}^n$. Note that this is equivalent to a non-minimal representation of $\mathfrak{E}_{\bar{E}}$,which has dimension $n-1$. Then, we can use the standard Euclidean projection $m_e$to the unit sphere, which is in turn mapped in S^{n-1}through the inverse natural embedding

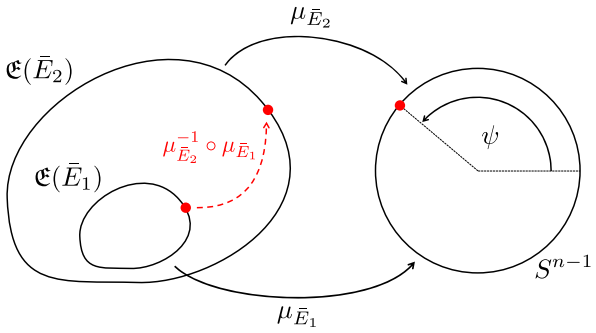

Fig. 14. The two manifolds $\mathfrak{E}(\bar{E}_1)$and $\mathfrak{E}(\bar{E}_2)$are level sets of $\mathcal{V}(p)$. We assume that they are diffeomorphic to the sphere S^{n-1}through the maps $\mu_{\bar{E}_1}$and $\mu_{\bar{E}_2}$. In this way points on the two manifolds can be associated pairwise by $\mu_{\bar{E}_2}^{-1} \circ \mu_{\bar{E}_1}$,and represented by the coordinate vector $\psi \in \mathbb{R}^{n-1}$.

$\Sigma_S^{-1} \mu_{\bar{E}} : \mathfrak{E}_{\bar{E}} \mapsto \Sigma_S^{-1} \circ m_e \circ \Phi(\mathfrak{E}_{\bar{E}})$. In order for this $\mu$to be a bijection, $\Phi(\mathfrak{E}_{\bar{E}})$must be a star domain for all $\bar{E}$. Hereinafter, we will use a $\mu_{\bar{E}}$so constructed, and we will equip $S^{n-1}$with the metrics inherited by the Euclidean $n-$ − dimensional space. Note that $\mu_{\bar{E}}$is constant on the eigenspace *ES*. This justifies to look at how close $\mu_{\bar{E}_1}(p_1)$and $\mu_{\bar{E}_2}(p_2)$are, as a way of checking if two evolutions are part of the same eigenmanifold.

8.2. Numerical representation of the eigenmanifold

By construction, the eigenmanifold $\mathfrak{M}$is unequivocally specified by its generator $\mathfrak{R}$, through the operator *G*. We can represented and store $\mathfrak{R}$numerically by discretizing it into a set of points $p_i \in \pi_{\mathfrak{X}}(\mathfrak{R})$. To be able to store them into a data structure we must express them in coordinates.

We identify a point $(p, 0)$ in $\Sigma_{\mathfrak{X}} \circ \mathfrak{R}$as $(\bar{E}, \psi) \in \mathbb{R}^n$. We use $\bar{E} \in \mathbb{R}^+$to select an energy level. This is completed by $\psi = \Lambda \circ \mu_{\bar{E}}(p) \in \mathbb{R}^{n-1}$which identifies a point on the sphere, with Λ chart (or an atlas) of S^{n-1}. To conclude, we represent the $j-$ − th manifold $\mathfrak{M}$as

- a scalar energy increment $\delta_E > 0$,
- a matrix $R_j \in \mathbb{R}^{\frac{E_{\max}}{\delta_E} \times (n-1)}$,collecting the coordinates of points of S^{n-1},

where $E_{\max}$ is the maximum energy that we are considering, and it is without loss of generality a multiple of δ_E. Considering the energy of the equilibrium to be 0, the $i-$ − th point in $\mathfrak{R}$can be retrieved from $R_j[i]$ - i. e. the $i-$ − th row of R_j- by means of $\Lambda^{-1}$and μ. The corresponding nonlinear mode is $\gamma_{(p_i,0)}$, and it can be retrieved by simulating (4). We store all R_j in the data structure R shown in Fig. 15.

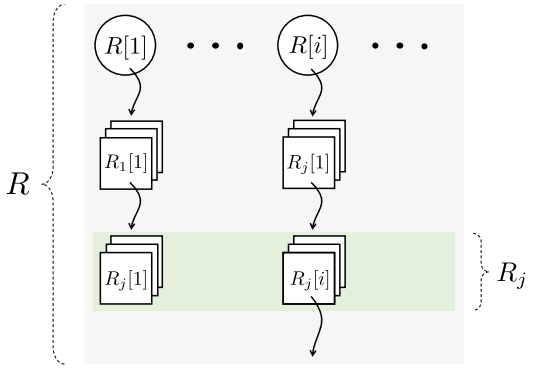

Fig. 15. Data structure R used to store a numerical description of all the generators of a given system. The state of the structure is the one that we can expect as output of Algorithm 1. The matrix R_j is the description of the $j-$ th generator $\mathfrak{R}$.

8.3. Finding the modes: exhaustive search

Leveraging on the discussed spherical representation, we introduce Algorithm 1, which exhaustively searches the entire configuration space for modes. The key idea here is to (a) iteratively look at a grid of points on the sphere S^{n-1} for each energy level, (b) store points that are associated to periodic and line-shaped evolutions, (c) connect the stored points using the metrics defined on S^{n-1}.

More specifically, Algorithm 1 starts by spanning $\mathfrak{X}$ increasing the energy from 0 to $E_{\max}$ with a step δ_E (line 3). All energy levels are exhaustively investigated by looking at all points represented by a dense enough lattice of S^{n-1} (line 7). The function isPeriodic$(\psi, \bar{E})$ simulates the evolution of the system from the initial condition $(\mu_{\bar{E}}^{-1} \circ \Lambda^{-1}(\psi), 0)$ and checks if it is periodic - i.e. condition (i) in Definition 7. In our implementation, we do that by evaluating the auto-correlation of the evolution, and by checking that at least one local maximum exists with value higher than 99% of the norm of the signal. Similarly notSelftIntersect$(\psi, \bar{E})$ simulates and checks for self-intersections - condition (ii) in Definition 7. If both conditions are true, the oscillation is a good candidate for being a mode, and can be stored (line 11). Before doing that, we check if the configuration associated to the other end of the oscillation has already been stored in a list (line 10). The energy spectrum is spanned again backwards to order points across levels, so that the point at position j in the $i-$ th list is as close as possible to the point at the same position in the $(i+1)$th list. Note that the two points are compared as elements of S^{n-1}, in this way getting rid of the energy dimension. This is implemented by findCloser$(R[i-1], \psi_1, \psi_2)$, which finds the element ψ in $R[i-1]$ which is closer to either ψ_1 or ψ_2. In case all points are farther than a certain threshold, the function returns the empty set. At the end of this process all the j–elements can be taken as representing the generator $\mathfrak{R}$ of a separate mode, for all $j \leq$ length$(R[1])$. Finally, note that in case the grid on S^{n-1} is not dense enough, the output of this algorithm may require some local refinement - either by hand or through a local optimization as discussed in the next subsection.

1: $E \leftarrow 0$
2: $i \leftarrow 0$
3: **while** $\bar{E} + \delta_E < E_{\max}$ **do**
4: $\quad \bar{E} \leftarrow \bar{E} + \delta_E$
5: $\quad i \leftarrow i + 1$
6: $\quad R[i] \leftarrow \{\}$
7: $\quad$ **for all** $\psi \in$ Grid(S^{n-1}) **do**
8: $\quad\quad$ **if** isPeriodic$(\psi, \bar{E})$ **then**
9: $\quad\quad\quad$ **if** notSelfIntersect$(\psi, \bar{E})$ **then**
10: $\quad\quad\quad\quad$ **if** findOtherEnd$(\psi, \bar{E}) \notin R[i]$ **then**
11: $\quad\quad\quad\quad\quad R[i] \leftarrow$ append$(R[i], \psi)$
12: **while** $i > 2$ **do**
13: $\quad j \leftarrow 0$
14: $\quad r_{\text{supp}} \leftarrow \{\}$
15: $\quad$ **while** $j \leq$ length$(R[i])$ **do**
16: $\quad\quad j \leftarrow j + 1$
17: $\quad\quad \psi_1 \leftarrow R_j[i]$
18: $\quad\quad \psi_2 \leftarrow$ findOtherEnd(ψ_1)
19: $\quad\quad \psi_c \leftarrow$ findCloser$(R[i-1], \psi_1, \psi_2)$
20: $\quad\quad r_{\text{supp}} \leftarrow$ append$(r_{\text{supp}}, \psi_c)$
21: $\quad R[i-1] \leftarrow r_{\text{supp}}$
22: $\quad i \leftarrow i - 1$
23: **return** R

Algorithm 1. Exhaustive search.

8.4. Finding the modes: prolonging linear modes

We say that $\mathfrak{M}$ is a prolongation of a linear eigenspace if for small oscillations around and equilibrium the behavior of the system is similar to the behavior of the linearized system at the same point. This can be formalized by asking that $T_{(p_{eq},0)}\mathfrak{M} = ES$, where ES is an eigenspace of the linearized system at the equilibrium configuration. Note that the equality sign is to be understood as between elements of RP^1, i.e. real projective spaces of dimension 1. This comparison is valid since $T_{(p,0)}\mathfrak{M}$ and ES are both subspaces of $\mathbb{R}^{2n}$ of dimension 2.

In case we are interested in finding only the $\mathfrak{R}$ generating an eigenmanifold which is a prolongation of the eigenspace ES, we can formulate the search procedure in a relatively straightforward way. We report the pseudo-code of this procedure in Algorithm 2 (where we dropped the subscript j from R_j since a single manifold is considered here).

As for the previous subsection, we rely on the sphere projection $\mu_{\bar{E}}$ to connect points placed on different energy levels. Here, the point ψ_{old} evaluated for $\bar{E}$, is used as initial condition of an optimization routine (findLocalMinimum) that searches for the closest periodic orbit by optimizing the degree of periodicity of the curve. This step of the algorithm falls into the class of shooting methods (Peeters et al., 2009). We consider here the maximum of the autocorrelation of the evolution as measure of periodicity.

Note that contrary to Algorithm 1, this procedure is not ensured to find a mode. For example, there is not explicit check that at each step we end up on an evolution which verifies conditions (i) and (ii) of Definition 7. However, it proved to work well in the practice, although its performance will be formally evaluated in future work.

8.5. Example: double pendulum

Consider the double pendulum in Fig. 2(d). The system is subject to gravity, and it has a linear spring connected in parallel to the second joint. Its stiffness is k, and it is unloaded when the two links are such that $x_2 = \pi/2$.

Its energy expressed in joint coordinates is (7) with $M(x)$ equal to

$$\begin{bmatrix} m_1 l_1^2 + m_2(l_1 + l_2)^2 - 2m_2 l_1 l_2(1 - \cos(x_2)) & * \\ m_2\left(l_2^2 + l_1 l_2 \cos(x_2)\right) & m_2 l_2^2 \end{bmatrix},$$

and $V(x) = V^*(x) - V^*(x_{eq})$ with

$$V^*(x) = \frac{1}{2}\left(x_2 - \frac{\pi}{2}\right)^2 + l_1(m_1 + m_2)(1 - \cos(x_1)) + l_2 m_2(1 - \cos(x_1 + x_2)),$$

where l_1 and l_2 are the lengths of the two links. We consider in the following $k = 10, m_1 = 0.4, m_2 = 0.4, l_1 = 1, l_2 = 1$. The resulting equilibrium configuration is $x_{eq} = (-0.3930, 1.2655)$. The eigenspaces of the linearized system are are $ES_1 = \text{Span}\{(0.352, -0.936, 0, 0), (0, 0, 0.352, -0.936)\}$ and $ES_2 = \text{Span}\{(0.995, 0.103, 0, 0), (0, 0, 0.995, 0.103)\}$, evaluated as discussed in Section 2. As for all other examples considered in this paper, the two modes correspond to anti-phase and in-phase oscillations respectively.

We evaluate the continuations of the two linear modes by using Algorithm 2. We also double-check the results by using Algorithm 1, which

1: $\psi_{\text{old}} \leftarrow \Lambda \circ \Sigma_S^{-1}\left(\frac{v}{\|v\|}\right), v \in ES$
2: $\bar{E} \leftarrow 0$
3: **while** $\bar{E} + \delta_E < E_{\max}$ **do**
4: $\quad \bar{E} \leftarrow \bar{E} + \delta_E$
5: $\quad R[i] \leftarrow$ findLocalMinimum$(\bar{E}, \psi_{\text{old}})$
6: $\quad \psi_{\text{old}} \leftarrow R[i]$
7: **return** R

Algorithm 2. Find Prolongation.

we use to identify other regular oscillations as well. Fig. 16 shows the result of this analysis. The configuraiton component of two generators $\pi_{\mathfrak{X}}(\Re)$extending the eigenspaces (dashed black lines) are shown with a purple and a yellow solid line. In accordance with Definition 7, they both start from the equilibrium x_{eq}. Some examples of modal evolutions extending the anti-phase linear mode are shown in Fig. 17(b). The oscillations are quite superimposed – even if not exactly. They are also quite close to the linear mode. In our experience, it is often the case that one of the two linear modes of a 2–DoF system is extended into such a quasi-strict nonlinear mode. This can be understood by looking at the dynamics in center of mass coordinates. A mode oscillating mostly in the radial direction will not be strongly affected by Coriolis and centrifugal forces, therefore showing a weak dependency on velocity.

An example of evolution of the anti-phase mode in Cartesian coordinates is shown in Fig. 18(a–d). Fig. 19(a,e,i) also report detailed account of the energy dependency of the Cartesian evolutions. As expected, this mode corresponds to a periodic compression-decompression motion of the double pendulum, and therefore to a mostly radial motion of the center of mass – which is placed in the middle of the second link.

Figs. 17 (a), 18(f-j), and 19(b,f,j) report instead examples of nonlinear modes extending the in-phase linear mode. This is a swing-like motion, and it is therefore more substantially affected by velocity-dependent actions. At low energies, the modal oscillations are close to the second linear mode. We can also recognize a small component along the first mode, with frequency of oscillation double the one of the main component. So, while swinging, the arm also goes through a small compression-decompression cycle. When the energy gets larger than 1J, the anti-phase component becomes bigger and bigger. It also self-resonates, i.e. two critical points within the period appear such that the velocity projected along the anti-phase eigenspace is zero. This is clearly visible in the Cartesian evolution of the second mass (see Fig. 19 (j)), which bounces up and down due to the marked compression-decompression component producing an s-shaped trejectory.

Interestingly, other two sets of non self-intersecting oscillations appear with a blue sky bifurcation at 1.2J, as shown in Fig. 16. One of the two oscillations disappears with the further increase of energy, while the other is present up to the maximum tested energy.

Note that these oscillations are individuated by Algorithm 1. They cannot be identified by Algorithm 2, since they are not a prolongation of

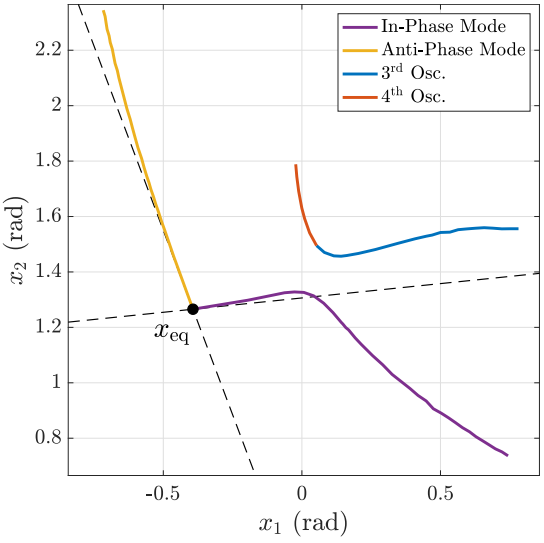

Fig. 16. Modal characterization of a double pendulum with parallel elasticity (see Fig. 2(d)). The figure shows the generators $\Re$for the two eigenmanifolds extending the in-phase and anti-phase linear modes. The corresponding eigenspaces are shown as black dashed lines. Two extra regular oscillations appear from the blue sky, for large enough energies. The set of points with zero velocity associated to these oscillations are shown as well.

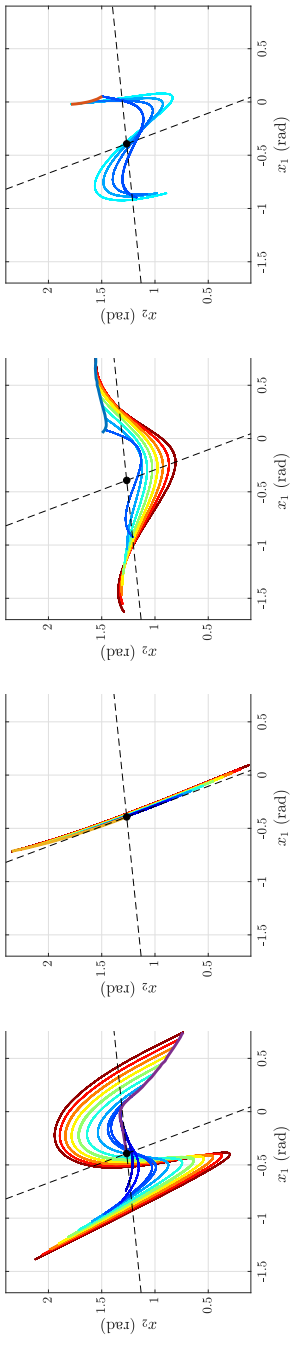

Fig. 17. Non-intersecting oscillations in the double pendulum with parallel elasticity (see Fig. 2(d)), expressed in joint coordinates. Panels (a,b) show examples of nonlinear modes, for several energy levels. Panels (c,d) report examples of the regular oscillations which are not nonlinear modes. The eigenspaces are shown as black dashed lines. Each panel also reports the corresponding generator as a solid line with the same color as in Fig. 16.

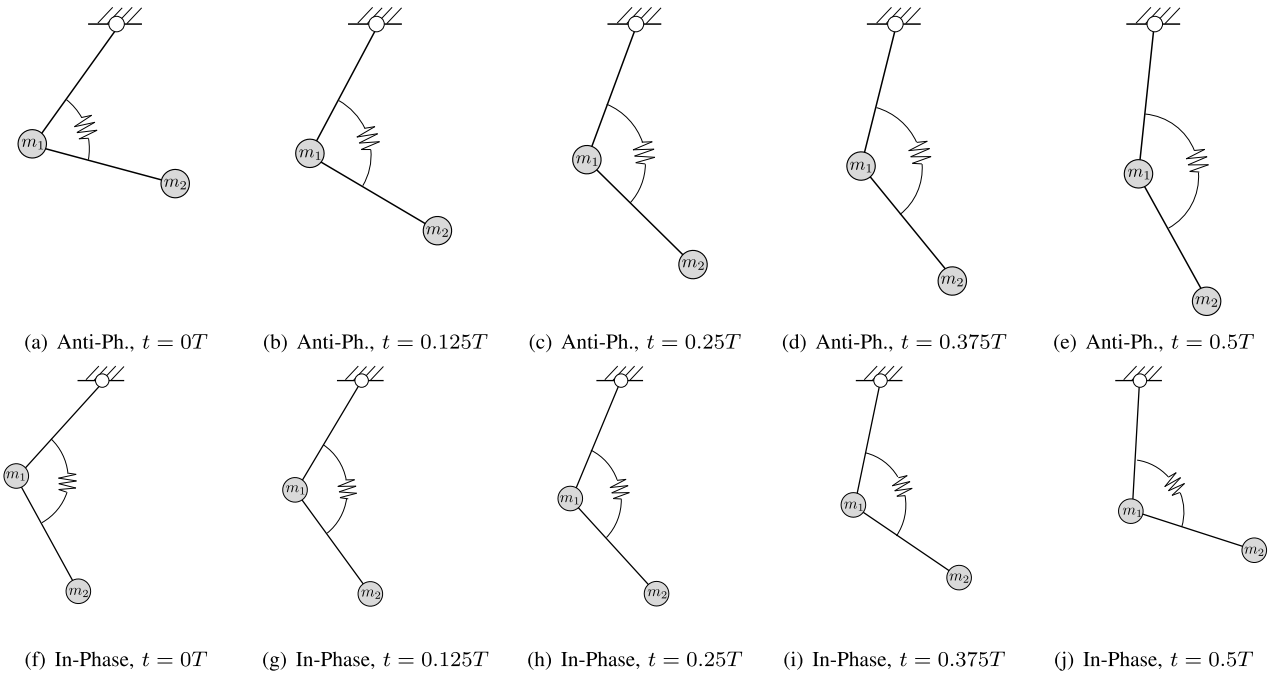

(a) Anti-Ph., $t = 0T$ (b) Anti-Ph., $t = 0.125T$ (c) Anti-Ph., $t = 0.25T$ (d) Anti-Ph., $t = 0.375T$ (e) Anti-Ph., $t = 0.5T$

(f) In-Phase, $t = 0T$ (g) In-Phase, $t = 0.125T$ (h) In-Phase, $t = 0.25T$ (i) In-Phase, $t = 0.375T$ (j) In-Phase, $t = 0.5T$

Fig. 18. Modal oscillations of the double pendulum with parallel elasticity (see Fig. 2(d)). Panels (a–e) show half a period for the anti phase mode. Panels (f–j) show half a period of an oscillation for the in phase mode. Note that this represent the behavior before the generator bends, and the self-resonance occurs. The second part of the oscillations repeats backward and it is therefore not shown. The gravity acceleration is not reported in the figure for the sake of clarity.

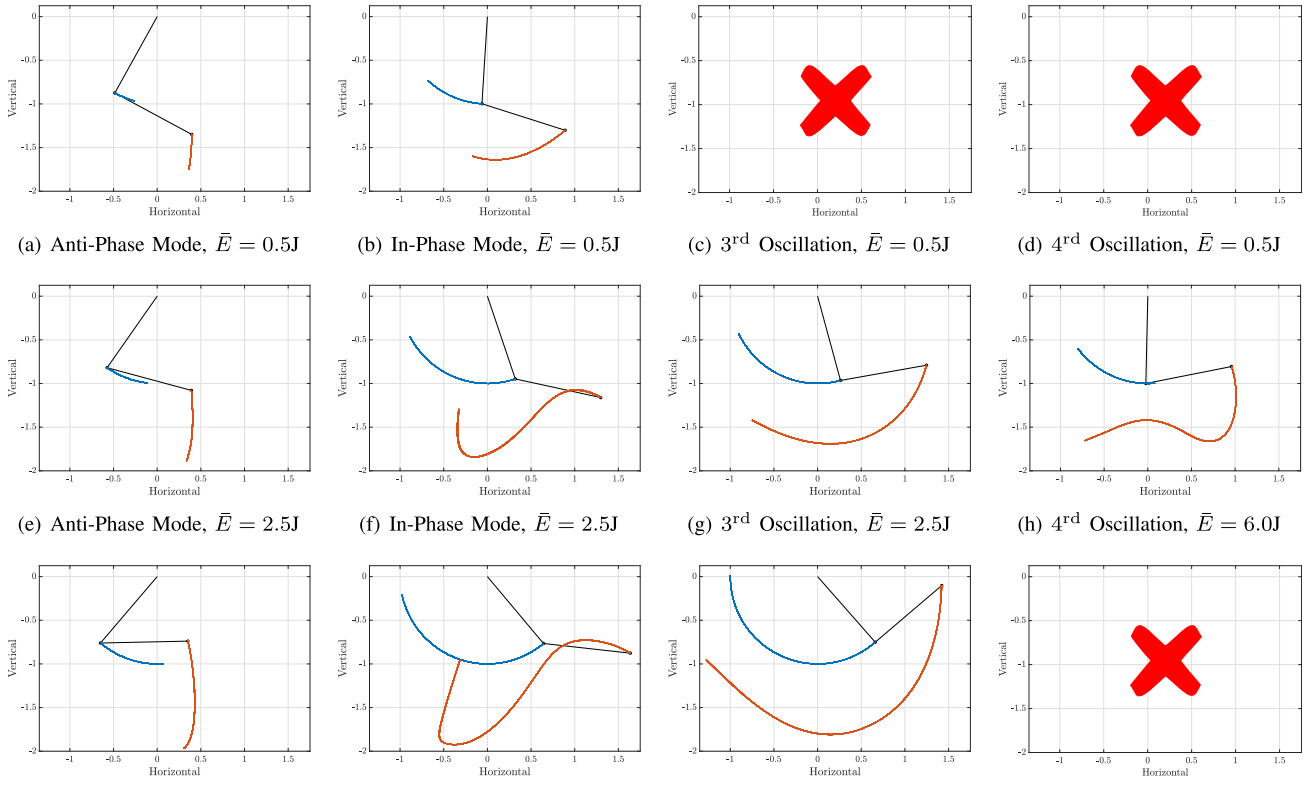

(a) Anti-Phase Mode, $\bar{E} = 0.5$J (b) In-Phase Mode, $\bar{E} = 0.5$J (c) 3^{rd} Oscillation, $\bar{E} = 0.5$J (d) 4^{rd} Oscillation, $\bar{E} = 0.5$J

(e) Anti-Phase Mode, $\bar{E} = 2.5$J (f) In-Phase Mode, $\bar{E} = 2.5$J (g) 3^{rd} Oscillation, $\bar{E} = 2.5$J (h) 4^{rd} Oscillation, $\bar{E} = 6.0$J

(i) Anti-Phase Mode, $\bar{E} = 6.0$J (j) In-Phase Mode, $\bar{E} = 6.0$J (k) 3^{rd} Oscillation, $\bar{E} = 6.0$J (l) 4^{rd} Oscillation, $\bar{E} = 6.0$J

Fig. 19. Nonlinear oscillations of a double pendulum with parallel elasticity (see Fig. 2(d)), for three energy levels. The mechanical system is shown in its initial condition (element of $\Re$). We also plot the trajectories of the two masses for 120 s of simulation. At 0.5J only the two nonlinear modes are present. The energy 2.5J is greater than the one in which the blue sky bifurcation happens, and the two extra line-shaped oscillations are present. Finally, one of the two extra oscillations is already disappeared at 6.0J.

any eigenspace, and the output of the algorithm does not even identify a generator since (x_{eq}, 0) is not contained in it. Nonetheless, they are interesting regular behaviors of the system in their own.

For example, consider the shape of the two sets in Fig. 16 for these two sets of oscillations, together with the generator of the in-phase mode prolongation. There is clearly an interval of energies (centered around 1.1J) within which the mode's generator bends, and its place is taken by the third set of oscillations. If an observer would look at the plot with this part covered, they would probably favour to associate the low energy part of the mode with the third set of oscillations, and the high energy part with the fourth set.

This cross-association is not an artifact of the proposed $\mathfrak{R}$representation. On the contrary, it is clearly identifiable while looking at the trajectories in coordinates. The trajectories in Fig. 17(c) are quite similar to the ones that the second mode manifests at low energies, and the ones in Fig. 17(d) matches very well the behavior of the same mode at high energies. The same effect can be observed in Cartesian evolutions. Fig. 19 (g and k) look like a continuation of Fig. 19 (b), and (f,j) a continuation of Fig. 19 (h).

Apart from being a quite peculiar (and exquisitely nonlinear) behavior, this also should warn on the perils of selecting a too large δ_E when using Algorithms 1 and 2. In this case the second mode would have been prolonged to the wrong set of oscillations.

9. Coordinate expressions of the embedding

Section 8 provides means of fully computing a description of an Eigenmanifold. However, this may be not enough in many applications where a compact functional representation of the manifold is needed for doing calculations. This section deals with producing such a description, by parameterizing the natural embedding of the eigenmanifold into the tangent bundle $\Sigma_{\mathfrak{M}} : \mathfrak{M} \hookrightarrow T\mathcal{X}$. This is a trivial mapping in its coordinate-free expression, connecting each point on the manifold to itself. However, its coordinate expression fully describes the manifold structure, as it will appear clear later.

Consider the charts $\Phi : U \to \mathbb{R}^n$and $\mathrm{d}\Phi_p : T_p\mathcal{X} \to \mathbb{R}^n$covering the open set $TU = \bigcup_{p\in U}\{p\} \times T_p\mathcal{X}$of $\mathcal{X}$, as introduced in Secs. 3 and .3. Similarly, consider $W \subset TU \cap \mathfrak{M}$, covered by the chart $\Xi : W \to \mathbb{R}^2$. We call $X : \mathbb{R}^2 \hookrightarrow \mathbb{R}^n$and $\dot{X} : \mathbb{R}^2 \hookrightarrow \mathbb{R}^n$the two functions such that

$$\left(X, \dot{X}\right) = (\Phi, \mathrm{d}\Phi) \circ \Sigma_{\mathfrak{M}} \circ \Xi^{-1}, \tag{38}$$

where we omitted the subscript of $\mathrm{d}\Phi_p$ for the sake of readability.

The two functions X and $\dot{X}$describe (locally) the modal manifold, mapping the coordinates of the Eigenmanifold into the configuration coordinates. Indeed, the Eigenmanifold can be directly defined in coordinates as

$$\mathfrak{M}_{\Phi\Xi} = \left\{(x, \dot{x}) \in \mathbb{R}^{2n}, \text{ s.t. } X - x = 0, \dot{X} - \dot{x} = 0\right\},$$

where we omitted the dependency of X and $\dot{X}$on the manifold parametrization. This definition clearly corresponds to the Rosenberg and Shaw-Pierre manifolds - as expressed by (25) and (33) respectively - and serves as their direct coordinate generalization.

Although this formulation is specific to the problem at hand, the use of coordinate expressions to describe embedded manifolds is common practice in computational geometry. Methods exist to automatically regress such a parametrization with few or null a priori information, as for example discussed in Krauskopf et al. (2006), Lin and Zha (2008), Wismüller, Verleysen, Aupetit, and Lee (2010) and McInnes, Healy, and Melville (2018). Nonetheless, finding parameterizations tailored on the eigenmanifold case is quite valuable, in order to build an intuition on the problem and to design effective algorithms.

9.1. Methods: estimating the manifold embedding

Consider as an example Algorithm 3. The key idea here is to (a) generate points of $\mathfrak{M}$, (b) for each of them evaluate examples of input-output pairs of $(X, \dot{X})$, and (c) fit the coordinate embedding from data.

As its very first action, the algorithm evaluates a generator by executing Algorithm 1 or 2 – referred as calculateGenerator(). Then, it evaluates all the associated modal evolution by direct simulation of system (6) – performed at line 8. The result of this step are samples of the coordinate expression of the modal evaluations $\Phi \circ \gamma_{(p_i,0)}$and $\mathrm{d}\Phi \circ \gamma'_{(p_i,0)}$, that we call $(x_{ev}, \dot{x}_{ev})$. These serve as example of outputs for $(X, \dot{X})$. We must now evaluate the corresponding inputs, so to get to a complete set of examples to be used to evaluate our functional approximation.

We can now evaluate the associated evolution of the parametrization in manifold coordinates ψ_{ev} by directly extracting salient characteristics from the state. This is implemented by extractParametrization$(x_{ev}, \dot{x}_{ev})$, which performs $\Xi \circ \pi_{\mathfrak{M}} \circ (\Phi, \mathrm{d}\Phi)^{-1}$, i.e. the inverse of (38). We introduce in the following two possible choices for this function.

Finally, $(X, \dot{X})$are estimated as the functions mapping all the ϕ_{ev} into all the $(x_{ev}, \dot{x}_{ev})$. These are collections of points in $\mathbb{R}^2$and $\mathbb{R}^{2n}$respectively. This can be done by using a state of the art interpolator (called interpolation(D) in the algorithm).

9.2. Energy parametrization

A natural choice comes from thinking of $\mathfrak{M}$as a fiber bundle with base space $\mathfrak{R}$. In this view, any point $(p^*, v^*) \in \mathfrak{M}$can be reached by first moving through $\mathfrak{R}$, and then continuing through the associated fiber (i.e. the orbit). This process is visually described by Fig. 20(a).

First, we want to parametrize the points in $\mathfrak{R}$. We already discussed in Section 7.2, that the potential energy of the points within the generator $\mathcal{E} \circ \Sigma_{\mathfrak{R}} : (p, 0) \mapsto \mathcal{V}(p)$can be used as a global chart for $\mathfrak{R}$.

The next step is to find a parametrization for the orbits expressed in the tangent bundle, i.e. each $G(\{p, 0\})$ such that $(p, 0) \in \mathfrak{R}$. Due to condition (i) in Definition 7, orbits have a S^1topology, and therefore they cannot be globally covered by a single chart. Still, we can cover all the orbit but a point by using arc length $\rho : S^1 \to \mathbb{R}$so defined

$$\rho : (p^*, v^*) \mapsto \int_0^{t^*} \mathcal{I}_{\gamma_{(p,0)}(t)}\left(\gamma'_{(p,0)}(t), \gamma'_{(p,0)}(t)\right) \mathrm{d}t, \tag{39}$$

where $\mathcal{I}$is the inertia tensor, t^* is the smallest positive value such that $(\gamma(t^*), \gamma'(t^*)) = (p^*, v^*)$, and (p, v) is the element in $\mathfrak{R}$verifying $\mathcal{E} \circ \Sigma_{\mathfrak{R}}(p, 0) = \mathcal{E} \circ \Sigma_{\mathfrak{M}}(p^*, v^*)$.

Note that global coverage can be achieved by creating an atlas defined by two charts. Consider the other end of the oscillation $\tilde{p} = \gamma_{(p,0)}(T/2)$, where T is the period of the oscillation. The atlas can be build by considering two charts defined similarly to (39). One starts from $(p, 0)$ and extends until $(\gamma_{(p,v)}(\epsilon + T/2), \gamma'_{(p,v)}(\epsilon + T/2))$, with ϵ being a small

1: $R \leftarrow$ calculateGenerator()
2: $D \leftarrow \{\}$
3: $\bar{E} \leftarrow 0$
4: $i \leftarrow 0$
5: **while** $\bar{E} + \delta_E < E_{max}$ **do**
6: $\quad \bar{E} \leftarrow \bar{E} + \delta_E$
7: $\quad i \leftarrow i + 1$
8: $\quad (x_{ev}, \dot{x}_{ev}) \leftarrow$ simulate$(R[i], \bar{E})$
9: $\quad \phi_{ev} \leftarrow$ extractParametrization$(x_{ev}, \dot{x}_{ev})$
10: $\quad D \leftarrow$ append$(D, \{\psi_{ev}, (x_{ev}, \dot{x}_{ev})\})$
11: **return** interpolate(D)

Algorithm 3. Find Eigenmanifold Embedding.

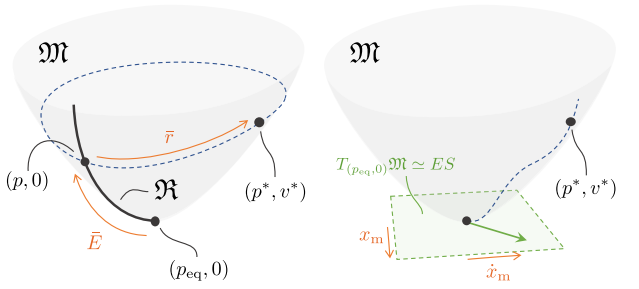

(a) Energy parametrization (b) Tangent parametrization

Fig. 20. Two parametrization strategies Ξ for a generic Eigenmanifold $\mathfrak{M} \subset T\mathfrak{X}$. In Panel (a), $\bar{E}$ is the energy of (p^*, v^*), and $\bar{r}$ is the length of the trajectory going from $(p, 0) \in \mathbb{R}$ to the target point, measured using the inertia tensor metrics (arch length). This is one possible chart for the orbit. The dotted line in Panel (b) is a geodesics of $\mathfrak{M}$ under the Sasaki metrics, passing through the equilibrium, with tangent vector $(x_{\text{m}}, \dot{x}_{\text{m}})$. The point (p^*, v^*) is the one reached by this trajectory after one second.

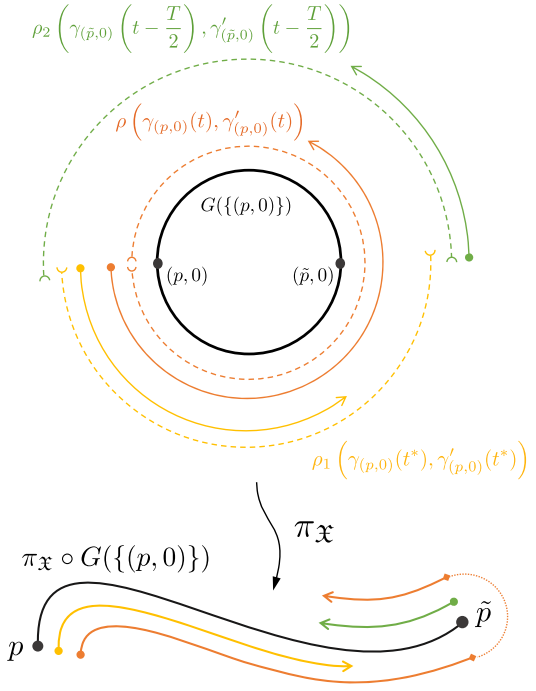

Fig. 21. Parameterizations of a single orbit $G(\{(p, 0)\})$, having S^1 topology, and being the collection of points assumed by the state evolution $(\gamma_{(p,0)}, \gamma'_{(p,0)})$. The top part of the picture shows the full view in $T\mathfrak{X}$, while the bottom part shows the behavior in configuration $\mathfrak{X}$. The points $(p,0) \in \mathfrak{R}$ and $(\tilde{p},0) \notin \mathfrak{R}$ are the only two cases in which the orbit reaches zero velocity. The associated configurations are therefore at the two ends of the line-shaped trajectory. The arc length ρ (red in figure) can be used to parametrize all the orbit but the point $(p, 0)$. This is represented by the dotted red line in figure. The arc lengths starting from $(p, 0)$ and $(\tilde{p}, 0)$ and extending only for half a cycle are also shown in figure, where they are referred as ρ_1 and ρ_2. Together, these two charts form an atlas. (For interpretation of the references to color in this figure legend, the reader is referred to the web version of this article.)

positive number. Viceversa, the other chart extends from $(\tilde{p}, 0)$ to $(\gamma_{(\tilde{p},v)}(\epsilon + T/2), \gamma'_{(\tilde{p},v)}(\epsilon + T/2))$. These two charts are called ρ_1 and ρ_2 respectively, and they are shown by Fig. 21. Together they cover the whole orbit $G(\{(p, 0)\})$. However, it is often convenient to work with a single chart, since dealing with more of them means having to take care of the switching from one chart to the other.

A third alternative is using a single non minimal representation. To this end, consider that the evolution is line-shaped in $\mathfrak{X}$- condition (ii) of Definition 7. Therefore, to identify a point (p^*, v^*) we only need to know where $p^* = \gamma_{(p,0)}(t^*)$ is along $\pi_{\mathfrak{X}} \circ G(\{(p,0)\})$. This can be measured using the arc length from p to p^*, or from $\tilde{p}$ to p^*. The first is equivalent to ρ_1 the second to ρ_2. Then the only information which is left to identify the point in $G(\{(p, 0)\})$ is the direction in which the system is traversing the trajectory - i.e. with velocity $\gamma'_{(p,0)}(t^*)$ or $\gamma'_{(\tilde{p},0)}(T/2 - t^*)$- which can be represented by a simple binary variable $s \in \{-1, 1\}$, that together with the arc length discussed above defines the non minimal parametrization. This can also be seen as s selecting the correct chart among the ρ_1 and ρ_2 defined above depending on the direction of v, therefore assuring that the coverage is actually global (see bottom part of Fig. 21).

Combining the charts for $\mathfrak{R}$ and S^1 we get $\Xi = (\mathcal{E} \circ \Sigma_{\mathfrak{R}}, \rho)$, which in turn leads to

$$\Xi \circ \pi_{\mathfrak{M}} \circ (\Phi, \mathrm{d}\Phi)^{-1} = (E, r), \tag{40}$$

where E is (7) and r is obtained by expressing (39) in coordinates

$$r : (x^*, \dot{x}^*) \mapsto \int_0^{t^*} \dot{x}^{\mathrm{T}} M(x) \dot{x} \, \mathrm{d}t, \tag{41}$$

where x is the solution of (6) such that $\dot{x}(0) = 0$ and $E(x, \dot{x}) = E(x^*, \dot{x}^*)$. The time t^* is the smallest positive value such that $(x(t^*), \dot{x}(t^*)) = (x^*, \dot{x}^*)$.

This results in the embeddings $X(\bar{E}, \bar{r}), \dot{X}(\bar{E}, \bar{r})$, where $\bar{E}$ is the orbit energy, and $\bar{r}$ is the position along the orbit. Note that this is a direct extension of the parametrization that we introduced for the Rosenberg case – Eq. (24). Indeed, the x_1 appearing there could be seen as an alternative parametrization for the orbit. Note that this choice covers in the best case only half of the orbit (see Fig. 21), since the additional velocity sign information is required to completely describe the motion. In fact, condition (ii) in Definition 7 implies that any configuration which is transited in one direction, will be transited also in the opposite one.

9.3. Example: double pendulum (Cont'd)

Consider the double pendulum introduced in Section 8.5. We apply Algorithm 3, with extractParametrization equal to (40). Applying the algorithm to the two nonlinear modes results in Fig. 22(a,b) and (c,d) respectively. Only X is shown for the sake of space. The interpolation is performed using `griddata` in `MatLab2019b`, set to interpolate linearly. The resulting approximation of manifold $\mathfrak{M}_{\Phi\Xi}$ is shown as a grey surface. Although being potentially *quasi-global*, the proposed parametrization $(\bar{E}, \bar{r})$ has the shortcoming of not defining an homeomorphism for any open neighborhood of the equilibrium configuration, since for each energy level there will always be at least a point not covered. This appears clear by looking at the examples of $\{(\bar{E}_{\text{ev}}, \bar{r}_{\text{ev}}), x_{\text{ev}}\}$ shown in colored solid lines in Fig. 22 (a–d). The closed orbit is opened by the parametrization and it appears here as a segment line. Its two ends refer to a same point in the real orbit, i.e. the initial condition.

9.4. Tangent parametrization

We introduce here a choice of parameters which is potentially more local than the one discussed in Section 9.2. Nonetheless, it has the great advantage of inducing a chart acting on an open set $W \subset \mathfrak{M}$ containing $(p_{\text{eq}}, 0)$. We assume here $\mathfrak{M}$ to be a prolongation of an eigenspace, i.e. $T_{(p_{\text{eq}},0)}\mathfrak{M} = \mathrm{Span}\{(c, 0), (0, c)\}$ for some $c \in \mathbb{R}^n$ (see Section 8.4).

Therefore, we can always construct $\Xi : W \to ES \simeq \mathbb{R}^2$, as the exponential map (Carmo, 1992, Sec 3.2) of $\mathfrak{M}$ in $(p_{\text{eq}}, 0)$. Note indeed that the Eigenmanifold can be interpreted as a Riemannian manifold inheriting its metrics from $T\mathfrak{X}$. In turn, the tangent bundle inherits the so-called Sasaki metrics from $\mathfrak{X}$, see e.g. Gudmundsson and Kappos (2002). As discussed for the energy parametrization, a full atlas could be built by

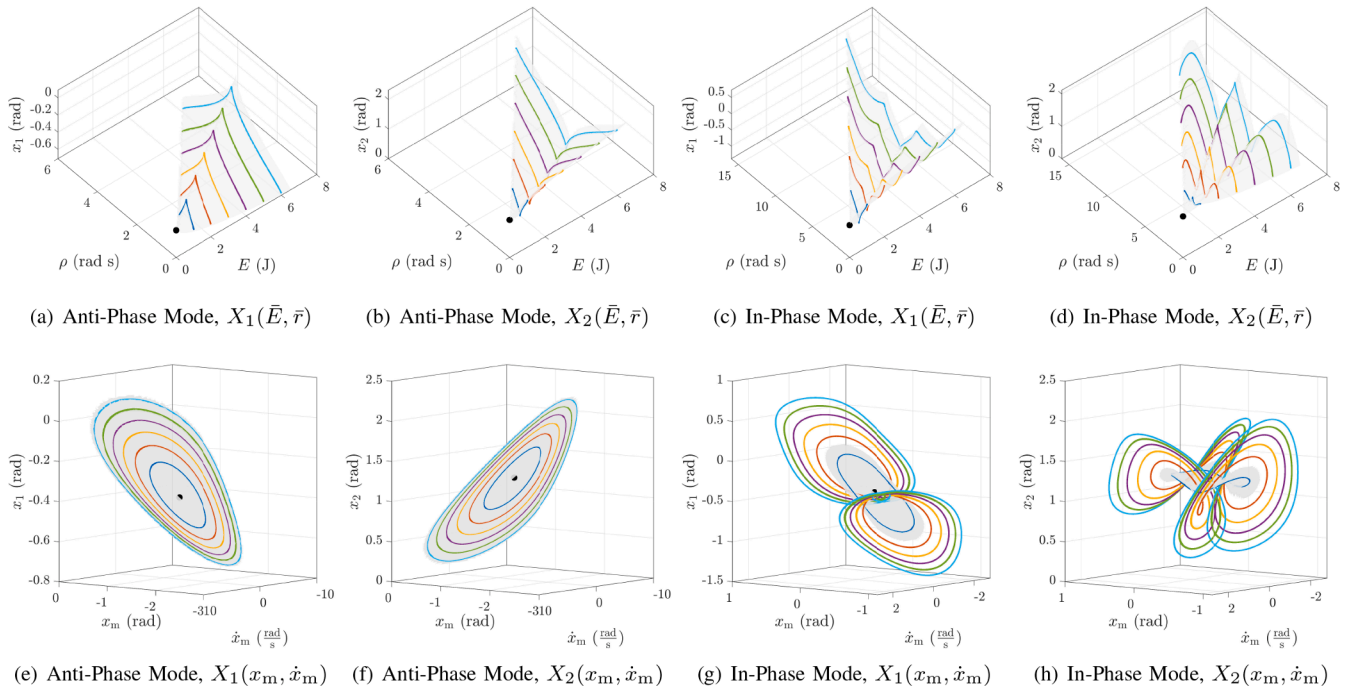

Fig. 22. Structure of the eigenmanifolds expressed using the energy (Panels (a–d)) and tangent (Panels (e–h)) parameterizations, for the double pendulum with parallel elasticity (see Fig. 2(d)). The extension of the anti-phase mode is reported in panels (a,b,e,f), and the one of the in-phase mode in panels (c,d,g,h). Only the configuration part is reported for the sake of space. The gray surface shows the eigenmanifold, as resulting from the parametrization obtained by modes interpolation. Five examples of modes (equidistant in energy) are shown with solid lines. The equilibrium is shown as well.

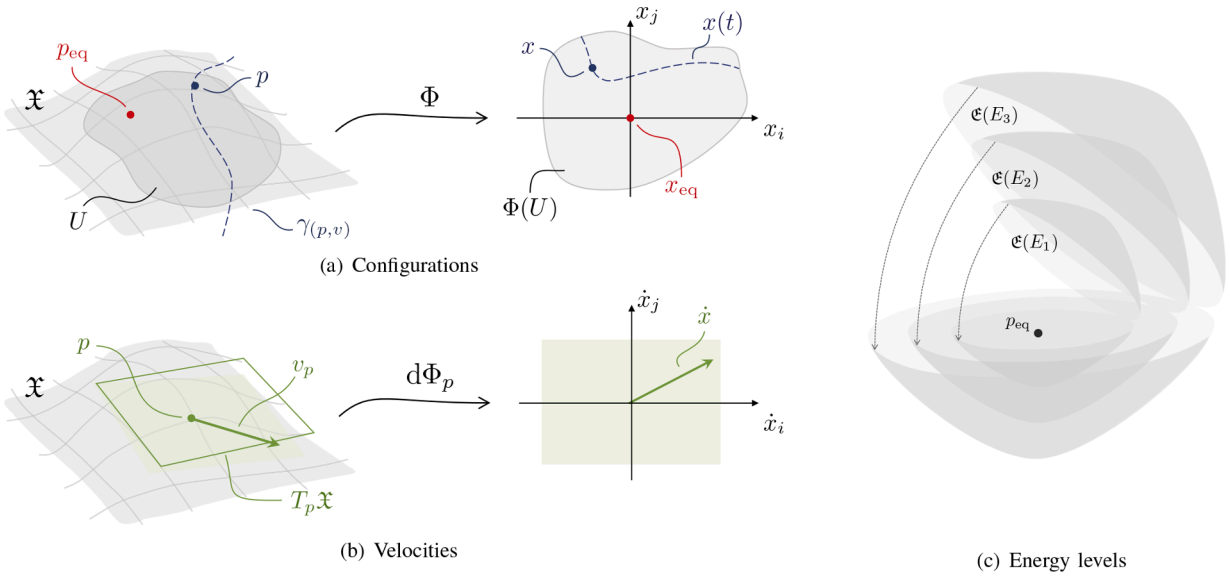

Fig. 23. Some standard differential geometry concepts used in the work to describe the dynamics on a nonlinear mechanical system - both in abstract geometrical settings (4) and in their relative coordinate expression (6). Panel (a) shows the configuration manifold $\mathfrak{X}$. Each point $p \in \mathfrak{X}$is a possible configuration for the mechanical system. p_eq is an isolated equilibrium of the system. An open set U is parametrized in coordinates through the chart Φ. Panel (b) depicts the tangent space $T_p\mathfrak{X} \simeq \mathbb{R}^n$in p. It contains all the possible velocities v_p that the system can have when being in configuraiton p. We will omit the subscript when not needed. The chart $\mathrm{d}\Phi_p$ maps all v_p in the coordinates derivatives $\dot{x}$. Together, $p$and v define the state of the mechanical system, and x and $\dot{x}$its coordinate expression. We indicate a trajectory of the system in coordinates starting from (p, v) as $\gamma_{(p,\,v)}$. We call $x(t) = \Phi \circ \gamma_{(p,v)}(t)$. Finally, Panel (c) shows the equi potential energy manifolds $\mathfrak{E} \subset \mathfrak{X}$, which are defined as the level sets of $\mathcal{V}(p)$. The manifolds are open in half in the figure, to clearly show that they are one contained in the other, and that the equilibrium configuration is at the center.

considering multiple charts. In this case the other charts could be selected by considering other tangent spaces to the Eigenmanifold.

This idea can be extended to more directly computable maps using retractions (Absil & Malick, 2012). The simplest retraction is the standard Euclidean projection of $\mathbb{R}^{2n}$into ES. Note that this map is chart dependent, i.e. changing $(\Phi, \mathrm{d}\Phi)$ generates different results. More sophisticated retractions will be considered in future work. We refer to the coefficients of x expressed in this bases as $x_\mathrm{m} = c^\mathrm{T}x$and $\dot{x}_\mathrm{m} = c^\mathrm{T}\dot{x}$. The function $\Xi \circ \pi_{\mathfrak{M}} \circ (\Phi, \mathrm{d}\Phi)^{-1}$is therefore the mapping $(x, \dot{x}) \mapsto (x_\mathrm{m}, \dot{x}_\mathrm{m})$. The coordinate expression of the embedding will therefore have the form

$X(x_m, \dot{x}_m)$and $\dot{X}(x_m, \dot{x}_m)$, which resemble the maps appearing in the ShawPierre case – Eq. (32).

9.5. Example: double pendulum (Cont'd)

Consider the double pendulum introduced in Section 8.5. We want to extract a description of the manifold using the tangent parametrization. This can be done by applying Algorithm 3, with extractParametrization implementing the Euclidean projection discussed above. We carry on the analysis for both the nonlinear modes identified in Section 8.5. Note that the anti-phase mode is projected through $c = (0.352, -0.936)$,while the in-phase through $c = (0.995, 0.103)$. Fig. 22(e,f) and (g,h) show the results for the anti-phase and the in-phase modes respectively. Only $X$is shown for the sake of space. Contrary to what happened with the other parameterization (Panels (a-d) in the same figure), the closed orbits are mapped here into closed curves.

To be coherent with Section 9.2, we interpolate the manifold using `griddata` in `MatLab2019b`, acting as a local linear interpolator. However, the smooth shape of the manifold expressed in these coordinates allows for using a much simpler interpolator. For example a fitting of a single third order multivariate polynomial would produce results almost indistinguishable from the more sophisticate local interpolation.

On the downside, the validity of the interpolation is more local. This is clear for the in-phase mode, for which the evolutions expressed as $(x_m, \dot{x}_m, x_1)$and $(x_m, \dot{x}_m, x_2)$start self intersecting for high energies. The eigenmanifold is therefore plotted only up to the energy in which this condition does not occur.

10. Discussions and conclusions

Nonlinear normal modes theory can provide to the control community an established vocabulary to discuss efficient motions in nonlinear mechanical systems, as well as a bag of mathematical tools to implement them. For example, we believe that very efficient oscillations can be implemented in mechanical system by identifying and stabilizing modal manifolds. As already discussed in the introduction, this can find possible use in robot locomotion and in industrial robotics, where the efficient execution of repetitive motions can lead to drastic reduction of production costs.

Invariant manifolds stabilization is a topic that received increasing attention in recent years. Standard output regulation techniques - as multivariate feedback linearization (Isidori, 2016) – can be seen as stabilizing the manifold identified by the level sets of the output. These techniques have been also extended to the hybrid case – see e.g. Westervelt, Grizzle, and Koditschek (2003). Immersion and Invariance is a control technique introduced in Astolfi and Ortega (2003), which aims at implementing low-order model matching through feedback stabilization of immersed invariant manifolds. This technique is used in Ortega, Yi, Romero, and Astolfi (2020) to achieve orbital stabilization. Virtual Holonomic constraints - defining an invariant manifold in configuration space (Maggiore & Consolini, 2012) - are imposed in Garofalo and Ott (2016) together with energy regulation, to obtain stable oscillation in serial elastic actuated robots. Transverse feedback linearization to stabilize controlled invariant submanifold is discussed in Nielsen and Maggiore (2008) and Shiriaev, Freidovich, and Gusev (2010). The stabilization of sumbanifolds is tackled in Montenbruck and Allgöwer (2016) in a coordinate-independent setting. All these techniques can be combined with modal analysis and used for Eigenmanifold stabilization.

As the main motivation of this work is to provide theoretical foundations for oscillation based locomotion, a few remarks on this application should be made. When in firm contact with the ground, a robot or biomechanical system can be well approximated by the model (4), (6). Locomotion, however, usually comprises stance and a flight phases, single or multi-leg ground contact, etc. This leads to hybrid nonlinear dynamical systems, having nonholonomic constraints and being underactuated in the flight phase. So one might wonder how the theory presented in this paper relates to the complex locomotion dynamics. Powerful tools in analysing and designing locomotion systems are given by low dimensional *template models* (Holmes, Full, Koditschek, & Guckenheimer, 2006). For example, extensive measurements of forces, elastic deformations and leg stiffness for different running and walking velocities revealed that running can be well characterized in a first approximation by a spring-loaded-inverted-pendulum, whose elasticity varies with running velocity (Blickhan, 1989; Schwind, 1998). The way in which this simple conceptual model, which assumes a linear massless leg, maps to the real segmented leg kinematics with distributed mass and to the complex tendon and muscle elastic properties, is still a topic of intensive research (Geyer et al., 2006; Seyfarth, & Van Leeuwen, 2000). Similarly, there exist multiple hypotheses and experimental evidence about energy efficiency mechanisms in walking, such as the gravitational pendulum effect of the swing leg and the catapult-like action of lower leg muscles and their tendons (Arampatzis, Brueggemann, & V., 1999; Collins, Wiggin, & G., 1989). We think that the concepts of nonlinear modes provide a powerful theoretical foundation for system and controller design in order to match the classical template models to full system dynamics.

Having to condensate in a few pages the results of more than a century of research coming from disparate communities, several aspects have been necessarily omitted, and of others we could only scratch the surface. Also, many questions still remain unanswered, and will required further substantial effort to be tackled. As an example, for what concerns the original Eigenmanifold definition provided here, some questions that will need careful analysis in the future are: (i) if at least n independent Eigenmanifolds exist for a generic nonlinear mechanical system; (ii) if they can be computed efficiently and which of the existing manifold learning techniques can be borrowed to this field; (iii) what happens when dissipation is introduced into the system, and if this makes the analysis harder or simpler; (iv) if simple control techniques can be devised to compensate the energy dissipation; and (v) how to extend these concept to the practically relevant case of hybrid underactuated or nonholonomic dynamics. To these and other questions we aim to provide answers in future work.

Declaration of Competing Interest

The authors declare that they have no known competing financial interests or personal relationships that could have appeared to influence the work reported in this paper.

Acknowledgments

This work is supported by European Union ERC project 835284 M-runners.

Notation: Appendix

A1. Fundamentals

We call $\mathfrak{X}$the configuration manifold of the robot. We consider it to be smooth and of dimension n. We call $\gamma : \mathbb{R} \to \mathfrak{X}$a curve in configuration space.

We call $T\mathfrak{X} = \bigcup_{p\in\mathfrak{X}}\{p\}\times T_p\mathfrak{X}$the tangent bundle of $\mathfrak{X}$- with $T_p\mathfrak{X}$tangent space of $\mathfrak{X}$in $p \in \mathfrak{X}$. The tangent bundle describes the state space of the robot. We consider in this work un-constrained systems, i.e. each element $(p, v_p) \in T\mathfrak{X}$is a possible state of the robot, with p configuration and v_p velocity. $\gamma' : \mathbb{R}\to T_{\gamma(t)}\mathfrak{X}$is the tangent vector field of γ, or velocity of the curve. We will omit the subscripts to velocities in the rest of the paper. We introduce the tangent bundle projection $\pi_{\mathfrak{X}} : T\mathfrak{X}\to\mathfrak{X}$such that $(p, v_p)\mapsto p$. Given the system kinematic description (not formalized here for the sake of space) and and the inertia properties of each body, the inertia tensor $\mathcal{I}_p : T_p\mathfrak{X}\times T_p\mathfrak{X}\to\mathbb{R}$is unequivocally specified as the positive-defined $(0,2) - -$ tensor such that $\mathcal{K}(p,v) = \frac{1}{2}\mathcal{I}_p(v,v)$is the kinetic energy of the robot. $\mathcal{I}_p$defines a metric on $\mathfrak{X}$called kinetic energy metric - making $(\mathfrak{X},\mathcal{I}_p)$a Riemann manifold, with associated Levi-Civita affine connection $\nabla_u v$. Conservative actions are introduced as derivatives of a potential $\nabla\mathcal{V} : \mathfrak{X}\to T^*\mathfrak{X}$, where $\mathcal{V} : \mathfrak{X}\to\mathbb{R}$is semi-positive definite. The total energy of the nonlinear mechanical system is $\mathcal{E} : T\mathfrak{X}\to\mathbb{R}$is the map $(p,v)\mapsto\mathcal{K}(p,v)+\mathcal{V}(p)$. Finally, all the submanifolds $\mathfrak{N}$of a manifold $\mathfrak{B}$that are considered in this paper are by construction embedded submanifolds. We call the associated natural embedding $\Sigma_{\mathfrak{N}} : \mathfrak{N}\to\mathfrak{B}$.

A2. Dynamics

The dynamics of a multi-body conservative system is (4). A curve $\gamma : \mathbb{R}\to\mathfrak{X}$is called integral curve (or a solution) of the dynamics if (γ, γ') satisfies (4). With an overloading of notation, we refer to the flow of the robot's dynamics as $\gamma_{(p,v)}(t) : \mathbb{R}\times T\mathfrak{X}\to\mathfrak{X}$. This is the integral curve of (4)such that $\gamma_{(p,v)}(0) = p$and $\gamma'_{(p,v)}(0) = v$. We say that $\gamma_{(p,\ v)}(t)$ is $T - -$ periodic if $\gamma_{(p,v)}(t) = \gamma_{(p,v)}(t+T)$for all t.

A3. Coordinates

For all open sets $U \in \mathfrak{X}$, an homeomorphism $\Phi : U\to\Phi(U)\subseteq\mathbb{R}^n$, i.e. a continuous function with continuous inverse, is considered. We call it coordinate chart of $\mathfrak{X}$in U, and we refer to points $x \in \Phi(U)$ as configuration coordinates. The coordinate chart also induces the homeomorphisms $\mathrm{d}\Phi_p : T_p\mathfrak{X}\to\mathbb{R}^n$, such that $(\Phi(p), \mathrm{d}\Phi_p(v)) = (x,\dot{x})$. The dot indicates a standard time derivative. The application of these charts to (4)yields the coordinate expression of the dynamics (6).

A4. Auxiliary operator

For the sake of conciseness of notation we define the dynamic flow operator acting on a subset S of $T\mathfrak{X}$as

$$G : S\mapsto \bigcup_{(p,v)\in S}\left\{\left(\gamma_{(p,v)}, \gamma'_{(p,v)}\right)(t), \forall t\in\mathbb{R}\right\}. \tag{42}$$

The set $G(S)$ contains all trajectories which which cross S. A set (or submanifold) is said to be invariant if it is a fixed point of G, i.e. $S = G(S)$. In other terms, all the trajectories passing through a point of $S$are fully contained in the set.

References

Absil, P.-A., & Malick, J. (2012). Projection-like retractions on matrix manifolds. *SIAM Journal on Optimization, 22*(1), 135–158.

Albu-Schaeffer, A., Lakatos, D., & Stramigioli, S. (2019). One-dimensional solution families of nonlinear systems characterized by scalar functions on Riemannian manifolds. arXiv:11911.01882,.

Arampatzis, A., Brueggemann, G. P., & V., M. (1999). The effect of speed on leg stiffness and joint kinetics in human running. *Journal of Biomechanics, 32*, 1349–1353.

Arnold, I. V. (1989). *Mathematical methods of classical mechanics*. New York: Springer.

Astolfi, A., & Ortega, R. (2003). Immersion and invariance: A new tool for stabilization and adaptive control of nonlinear systems. *IEEE Transactions on Automatic control, 48* (4), 590–606.

Avramov, K. V., & Mikhlin, Y. V. (2013). Review of applications of nonlinear normal modes for vibrating mechanical systems. *Applied Mechanics Reviews, 65*(2).

Benci, V. (1984). Normal modes of a lagrangian system constrained in a potential well, *1. Annales de l'institut henri poincare (c) non linear analysis* (pp. 379–400). Elsevier.

Birkhoff, G. D. (1917). Dynamical systems with two degrees of freedom. *Transactions of the American Mathematical Society, 18*, 199–300.

Blickhan, R. (1989). The spring-mass model for running and hopping. *Biomechanics, 22* (5), 1217–1227.

Bullo, F., & Lewis, A. D. (2004). *Geometric control of mechanical systems: Modeling, analysis, and design for simple mechanical control systems. 49*. Springer Science & Business Media.

Calzolari, D., Della Santina, C., & Albu-Schäffer, A. (2021). Pd-like regulation of mechanical systems with prescribed bounds of exponential stability: The point-to-point case. *IEEE Control Systems Letters*.

Carmo, M. P.d. (1992). *Riemannian geometry*. Birkhäuser.

Cirillo, G. I., Mauroy, A., Renson, L., Kerschen, G., & Sepulchre, R. (2016). A spectral characterization of nonlinear normal modes. *Journal of Sound and Vibration, 377*, 284–301.

Collins, S., Wiggin, B., & G., S. (1989). Reducing the energy cost of human walking using an unpowered exoskeleton. *SIAM Review, Society for Industrial and Applied Mathematic, 22*(5), 1217–1227.

Cristofaro-Gardiner, D., Hutchings, M., et al. (2016). From one reeb orbit to two. *Journal of Differential Geometry, 102*(1), 25–36.

De Luca, A., & Siciliano, B. (1991). Closed-form dynamic model of planar multilink lightweight robots. *IEEE Transactions on Systems, Man, and Cybernetics, 21*(4), 826–839.

Della Santina, C., & Albu-Schäffer, A. (2020). Differential analysis of nonlinear systems: Revisiting the pendulum example. *Submitted to American control conference (ACC), 2020 ieee annual conference on*. IEEE.

Della Santina, C., Catalano, M. G., & Bicchi, A. (2020). *Soft robots*. In M. H. Ang, O. Khatib, & B. Siciliano (Eds.). Berlin, Heidelberg: Springer.

Della Santina, C., Lakatos, D., Bicchi, A., & Albu-Schaeffer, A. (2019). Exact modal characterization of the non conservative non linear radial mass spring system. *2019 international conference on robotics and automation (ICRA)* (pp. 3101–3107). IEEE.

Ekeland, I., & Hofer, H. (1987). Convex hamiltonian energy surfaces and their periodic trajectories. *Communications in Mathematical PHysics, 113*(3), 419–469.

Ekeland, I., & Lasry, J.-M. (1980). On the number of periodic trajectories for a hamiltonian flow on a convex energy surface. *Annals of Mathematics*, 283–319.

Gabale, A. P., & Sinha, S. (2011). Model reduction of nonlinear systems with external periodic excitations via construction of invariant manifolds. *Journal of Sound and Vibration, 330*(11), 2596–2607.

Garofalo, G., & Ott, C. (2016). Energy based limit cycle control of elastically actuated robots. *IEEE Transactions on Automatic Control, 62*(5), 2490–2497.

Gendelman, O., Manevitch, L., Vakakis, A. F., & M'closkey, R. (2001). Energy pumping in nonlinear mechanical oscillators: part I-dynamics of the underlying hamiltonian systems. *Journal of Applied Mechanics, 68*(1), 34–41.

Geyer, H., Seyfarth, A., & Blickhan, R. (2006). Compliant leg behaviour explains basic dynamics of walking and running. *Proceedings of the Royal Society B: Biological Sciences, 273*(1603), 2861–2867.

Giambó, R., Giannoni, F., & Piccione, P. (2020). *Multiple orthogonal geodesic chords and a proof of seifert's conjecture on brake orbits*.

Gluck, H., & Wolfgang, Z. (1983). Existence of periodic motions of conservative systems. *Seminar on Minimal Submanifolds*, 65–98.

Guckenheimer, J., & Holmes, P. (2013). *Nonlinear oscillations, dynamical systems, and bifurcations of vector fields. 42*. Springer Science & Business Media.

Gudmundsson, S., & Kappos, E. (2002). On the geometry of tangent bundles. *Expositiones Mathematicae, 20*(1), 1–41.

Halás, M., & Moog, C. H. (2013). Definition of eigenvalues for a nonlinear system. *IFAC Proceedings Volumes, 46*(23), 600–605.

Haldane, D. W., Yim, J. K., & Fearing, R. S. (2017). Repetitive extreme-acceleration (14-g) spatial jumping with salto-1p. *2017 IEEE/RSJ international conference on intelligent robots and systems (IROS)* (pp. 3345–3351). IEEE.

Haller, G., & Ponsioen, S. (2016). Nonlinear normal modes and spectral submanifolds: existence, uniqueness and use in model reduction. *Nonlinear Dynamics, 86*(3), 1493–1534.

Hill, T., Neild, S., & Cammarano, A. (2016a). An analytical approach for detecting isolated periodic solution branches in weakly nonlinear structures. *Journal of Sound and Vibration, 379*, 150–165.

Hill, T., Neild, S., Cammarano, A., & Wagg, D. (2016b). The influence of phase-locking on internal resonance from a nonlinear normal mode perspective. *Journal of Sound and Vibration, 379*, 135–149.

Hingston, N. (1993). On the growth of the number of closed geodesics on the two-sphere. *International Mathematics Research Notices, 1993*(9), 253–262.

Hogan, N., & Sternad, D. (2007). On rhythmic and discrete movements: Reflections, definitions and implications for motor control. *Experimental Brain Research, 181*(1), 13–30.

Holmes, P. (1986). Chaotic motions in a weakly nonlinear model for surface waves. *Journal of Fluid Mechanics, 162*, 365–388.

Holmes, P., Full, R., Koditschek, D., & Guckenheimer, J. (2006). The dynamics of legged locomotion: Models, analyses, and challenges. *SIAM Review, Society for Industrial and Applied Mathematic, 48*(2), 207–304.

Hong, D., Hill, T. L., & Neild, S. A. (2019). Conditions for the existence of isolated backbone curves. *Proceedings of the Royal Society A, 475*(2232), 20190374.

Horn, J. (1903). Beitrage zur theorie der kleinen schwingungen. *Zeitschrift fr Angewandte Mathematik und Physik, 48*, 400–434.

Hu, X., & Long, Y. (2002). Closed characteristics on non-degenerate star-shaped hypersurfaces in R 2n. *Science in China Series A: Mathematics, 45*(8), 1038.

Isidori, A. (2016). Lectures in feedback design for multivariable systems. *Advanced textbooks in control and signal processing*.

Jiang, D., Pierre, C., & Shaw, S. (2005). Nonlinear normal modes for vibratory systems under harmonic excitation. *Journal of Sound and Vibration, 288*(4), 791–812.

José, J., & Saletan, E. (2000). Classical dynamics: A contemporary approach.

Kawano, Y., & Ohtsuka, T. (2015). Stability criteria with nonlinear eigenvalues for diagonalizable nonlinear systems. *Systems & Control Letters, 86*, 41–47.

Kawano, Y., & Ohtsuka, T. (2017). Nonlinear eigenvalue approach to differential Riccati equations for contraction analysis. *IEEE Transactions on Automatic Control, 62*(12), 6497–6504.

Kerschen, G., Peeters, M., Golinval, J.-C., & Vakakis, A. F. (2009). Nonlinear normal modes, part I: A useful framework for the structural dynamicist. *Mechanical Systems and Signal Processing, 23*(1), 170–194.

Kokotovic, P., Khali, H. K., & O'reilly, J. (1999). *Singular perturbation methods in control: Analysis and design. 25*. Siam.

Koopman, B. O. (1931). Hamiltonian systems and transformation in hilbert space. *Proceedings of the National Academy of Sciences of the United States of America, 17*(5), 315.

Krauskopf, B., Osinga, H. M., Doedel, E. J., Henderson, M. E., Guckenheimer, J., Vladimirsky, A., … Junge, O. (2006). A survey of methods for computing (un) stable manifolds of vector fields. *Modeling and computations in dynamical systems: In commemoration of the 100th anniversary of the birth of John von Neumann* (pp. 67–95). World Scientific.

Kumar, K. R., & Narayanan, S. (2008). Active vibration control of beams with optimal placement of piezoelectric sensor/actuator pairs. *Smart Materials and Structures, 17*(5), 055008.

Kvalheim, M. D., & Bloch, A. M. (2019). Families of periodic orbits: Closed 1-forms and global continuability. arXiv:1906.03528,.

Lakatos, D., Friedl, W., & Albu-Schäffer, A. (2017). Eigenmodes of nonlinear dynamics: Definition, existence, and embodiment into legged robots with elastic elements. *IEEE Robotics and Automation Letters, 2*(2), 1062–1069.

Li, J. (2003). Hilbert's 16th problem and bifurcations of planar polynomial vector fields. *International Journal of Bifurcation and Chaos, 13*(01), 47–106.

Lin, T., & Zha, H. (2008). Riemannian manifold learning. *IEEE Transactions on Pattern Analysis and Machine Intelligence, 30*(5), 796–809.

Liu, C.-g., Long, Y., & Zhu, C. (2002). Multiplicity of closed characteristics on symmetric convex hypersurfaces in $\mathbb{R}^{2n}$. *Mathematische Annalen, 323*(2), 201–215.

Long, Y., & Zhu, C. (2002). Closed characteristics on compact convex hypersurfaces in R2n. *Annals of Mathematics*, 317–368.

Lyapunov, A. (1907). Problème général de la stabilité du mouvement, *9*. *Annales de la faculté des sciences de toulouse: Mathématiques* (pp. 203–474).

Maggiore, M., & Consolini, L. (2012). Virtual holonomic constraints for euler–lagrange systems. *IEEE Transactions on Automatic Control, 58*(4), 1001–1008.

McInnes, L., Healy, J., & Melville, J. (2018). Umap: Uniform manifold approximation and projection for dimension reduction. arXiv:1802.03426,.

Mezić, I. (2005). Spectral properties of dynamical systems, model reduction and decompositions. *Nonlinear Dynamics, 41*(1–3), 309–325.

Montenbruck, J. M., & Allgöwer, F. (2016). Asymptotic stabilization of submanifolds embedded in riemannian manifolds. *Automatica, 74*, 349–359.

Moser, J. (1976). Periodic orbits near an equilibrium and a theorem by Alan Weinstein. *Communications on Pure and Applied Mathematics, 29*(6), 727–747.

Nayfeh, A. H. (2008). *Perturbation methods*. John Wiley & Sons.

Neild, S. A., Champneys, A. R., Wagg, D. J., Hill, T. L., & Cammarano, A. (2015). The use of normal forms for analysing nonlinear mechanical vibrations. *Philosophical Transactions of the Royal Society A: Mathematical, Physical and Engineering Sciences, 373*(2051), 20140404.

Nielsen, C., & Maggiore, M. (2008). On local transverse feedback linearization. *SIAM Journal on Control and Optimization, 47*(5), 2227–2250.

Noël, J.-P., & Kerschen, G. (2017). Nonlinear system identification in structural dynamics: 10 more years of progress. *Mechanical Systems and Signal Processing, 83*, 2–35.

Oñate, E. (2013). *Structural analysis with the finite element method. Linear statics: Volume 2: beams, plates and shells*. Springer Science & Business Media.

Ortega, R., Yi, B., Romero, J. G., & Astolfi, A. (2020). Orbital stabilization of nonlinear systems via the immersion and invariance technique. *International Journal of Robust and Nonlinear Control, 30*(5), 1850–1871.

Padoan, A., & Astolfi, A. (2019). Singularities and moments of nonlinear systems. *IEEE Transactions on Automatic Control*.

Peeters, M., Viguié, R., Sérandour, G., Kerschen, G., & Golinval, J.-C. (2009). Nonlinear normal modes, part ii: Toward a practical computation using numerical continuation techniques. *Mechanical Systems and Signal Processing, 23*(1), 195–216.

Pesheck, E., Pierre, C., & Shaw, S. (2002). A new Galerkin-based approach for accurate non-linear normal modes through invariant manifolds. *Journal of Sound and Vibration, 249*(5), 971–993.

Pikovsky, A., Kurths, J., Rosenblum, M., & Kurths, J. (2003). *Synchronization: A universal concept in nonlinear sciences. 12*. Cambridge university press.

Poincaré, H. (1899). *Les méthodes nouvelles de la mécanique céleste. 3*. Gauthier-Villars et fils.

Rabinowitz, P. H. (1977). Periodic solutions of Hamiltonian systems.. *Technical Report*. WISCONSIN UNIV MADISON MATHEMATICS RESEARCH CENTER.

Renson, L., Kerschen, G., & Cochelin, B. (2016). Numerical computation of nonlinear normal modes in mechanical engineering. *Journal of Sound and Vibration, 364*, 177–206.

Roberts, T. J., & Azizi, E. (2011). Flexible mechanisms: The diverse roles of biological springs in vertebrate movement. *Journal of Experimental Biology, 214*(3), 353–361.

Robinson, D. W., Pratt, J. E., Paluska, D. J., & Pratt, G. A. (1999). Series elastic actuator development for a biomimetic walking robot. *1999 IEEE/ASME international conference on advanced intelligent mechatronics (cat. no. 99th8399)* (pp. 561–568). IEEE.

Rosenberg, R. (1966). On nonlinear vibrations of systems with many degrees of freedom. *Advances in Applied Mechanics, 9*, 155–242.

Rosenberg, R. M. (1960). Normal modes of nonlinear dual-mode systems.

Schaal, S., Sternad, D., Osu, R., & Kawato, M. (2004). Rhythmic arm movement is not discrete. *Nature Neuroscience, 7*(10), 1136–1143.

Schwind, W. (1998). *Spring loaded inverted pendulum running: A plant model*. Univ. of Michigan. PhD thesis.

Seifert, H. (1948). Periodic movements of mechanical systems. *mathematical journal, 51*(2), 197–216.

Seyfarth, A., R., B., & Van Leeuwen, J. L. (2000). Optimum take-off techniques and muscle design for long jump. *The Journal of Experimental Biology, 203*(5), 741–750.1

Shaw, S. W., & Pierre, C. (1993). Normal modes for non-linear vibratory systems. *Journal of Sound and Vibration, 164*(1), 85–124.

Shaw, S. W., & Pierre, C. (1994). Normal modes of vibration for non-linear continuous systems. *Journal of Sound and Vibration, 169*(3), 319–347.

Shiriaev, A. S., Freidovich, L. B., & Gusev, S. V. (2010). Transverse linearization for controlled mechanical systems with several passive degrees of freedom. *IEEE Transactions on Automatic Control, 55*(4), 893–906.

Szalai, R., Ehrhardt, D., & Haller, G. (2017). Nonlinear model identification and spectral submanifolds for multi-degree-of-freedom mechanical vibrations. *Proceedings of the Royal Society A: Mathematical, Physical and Engineering Sciences, 473*(2202), 20160759.

Tedrake, R., Zhang, T. W., Fong, M.-f., & Seung, H. S. (2004). Actuating a simple 3d passive dynamic walker, *5*. *Ieee international conference on robotics and automation, 2004. proceedings. ICRA'04. 2004* (pp. 4656–4661). IEEE.

Wang, F., Bajaj, A. K., & Kamiya, K. (2005). Nonlinear normal modes and their bifurcations for an inertially coupled nonlinear conservative system. *Nonlinear Dynamics, 42*(3), 233–265.

Wang, W., Hu, X., Long, Y., et al. (2007). Resonance identity, stability, and multiplicity of closed characteristics on compact convex hypersurfaces. *Duke Mathematical Journal, 139*(3), 411–462.

Weinstein, A. (1973). Normal modes for nonlinear hamiltonian systems. *Inventiones Mathematicae, 20*(1), 47–57.

Westervelt, E. R., Grizzle, J. W., & Koditschek, D. E. (2003). Hybrid zero dynamics of planar biped walkers. *IEEE Transactions on Automatic Control, 48*(1), 42–56.

Williams, M. O., Kevrekidis, I. G., & Rowley, C. W. (2015). A data–driven approximation of the koopman operator: extending dynamic mode decomposition. *Journal of Nonlinear Science, 25*(6), 1307–1346.

Wismüller, A., Verleysen, M., Aupetit, M., & Lee, J. A. (2010). Recent advances in nonlinear dimensionality reduction, manifold and topological learning.. *ESANN*.